Progressive Damage and Crack Propagation Analysis of Composite-Patched Aluminum Plate with 3D Inclined Crack under Fatigue Loading

By:

Javad Eidan and Mohammad Zaman Kabir*
Department of Civil and Environmental Engineering, AmirKabir University of Technology, Tehran, Iran
***The corresponding author, Tel: 982164543032, email: mzkabir@aut.ac.ir

Abstract

Fatigue crack growth and damage of adhesive layer in a composite-patched aluminum plate with three dimensional inclined crack was simulated using Extended Finite Element Method (XFEM) and Cohesive Zone Model (CZM). A Python script was developed to model fatigue crack growth using XFEM in ABAQUS environment. Three adhesive materials and five patch lay-up sequences were considered to investigate the size and shape of damaged (debonded) region in different configurations. The effect of including damage in adhesive layer on global response of the structure and 3D crack geometry in metallic structure was studied. The interaction between crack growth in bulk material and damage in adhesive layer was discussed. It was concluded that neglecting damage in adhesive layer results in 8.4 to 23.2 percent overestimated fatigue life for different sample configuration. Smoother crack geometry was obtained from damage-including models with respect to models that do not include damage. Crack front shape was also highly affected, despite the fact that the effect on crack trajectory was not significant. It was also observed that in specimens with lower final strength and high ductility adhesive, structural response is resulted from an interaction between damage in adhesive and crack growth in bulk material.

Keywords:
Composite Reinforcement; adhesive; Fatigue life; crack trajectory

1. Introduction

Aluminum alloys are extensively employed in the aeronautics and maritime industries because of their beneficial properties, including low density, high strength, and good corrosion resistance. However, they are vulnerable to cracking in harsh operational environments [1].
Structural cracks have a significant negative impact on the structural integrity, flexibility, and fatigue life of engineered structures [2].

Fatigue is a major cause of failure in cracked structures that are subjected to cyclic loading [3].
Extending the service life of cracked components in the aerospace industry is a critical engineering challenge that has attracted significant research attention in recent decades [4, 5].

Fiber-reinforced polymer (FRP) composites are one of the most frequently used materials for strengthening of metallic structures against fatigue. Excellent mechanical properties of these materials make them an attractive selection for repairing and strengthening of structural components [6].

FRP composite patch extends fatigue life of cracked structure by reducing stress range around the crack and enhancing stress flow in cracked segment. stress is transferred to the patch from metallic substrate through bonded interface. The patch also bridges the crack and decreases the crack opening displacement [7].

The numerous advantages of adhesively bonded joints, compared to other more traditional joining methods, have led to their increased use in recent years across a variety of industries [8, 9]. Adhesive bonding technology is commonly utilized in multi-material connections between FRP and metal structures, as it can ensure the integrity of the adherends with reduced stress concentration, improved sealing properties, and enhanced durability [10].

In the case of cracked metallic structures composite patches are bonded to the structure using a thin layer of adhesive [11, 12] which plays an essential role in mechanical performance of the structure [13, 14]. Due to weakness in tension and shear, this layer is the most vulnerable part of the structure-adhesive-patch assembly in most loading cases [15]. Debonding of FRP patch from metallic substrate was observed during fatigue loading near the crack-tip [16].

Colombi et al. [17] tested steel plates with central holes and two initial cracks that were strengthened with carbon FRP (CFRP) composite patches on both sides. They reported that a semielliptical-shaped zone of debonding in the interface of steel and adhesive was observed. Finally, it was concluded that debonding of the patch has a significant influence on stress intensity factor (SIF) at crack tip and crack growth rate, respectively.

Sabelkin et al. [18] conducted experimental tests on 2024-T3 aluminum alloy panels with 12.7-mm-long and 3-mm-wide central notch. The aluminum panels were strengthened with patches of boron-epoxy composite, bonded on one side. The debonding region was limited to a slender ellipse along the crack with major axis equal to crack length, and approximately 2-mm minor axis.

Hosseini-Toudeshky et al. [19] simulated crack propagation of single-side adhesively bonded aluminum panels in general mixed mode conditions. The damage in adhesive layer was neglected in FE simulation model. However, numerical results were verified against experimental data.

Huawen et al. [20] conducted fatigue tests on double-edge-notched steel plates that were strengthened with prestressed CFRP laminates. Inspecting specimens after failure, they observed a trapezoidal-shaped region of debonding. The size of this region decreased with increasing prestress level of CFRP laminates.

Using cohesive zone method, Khoramishad et al. [21] developed a strain-based progressive damage model for adhesively bonded joints under fatigue loading which only depends on adhesive system and not related to joint configuration. A bilinear traction-separation response was used to represent the cohesive zone model (CZM) that was utilized to simulate the cohesive behavior of bonding adhesive. Additionally, a strain-based degrading formulation was developed to account for progressive deleterious effect of fatigue loading on mechanical characteristics of cohesive elements.

Kim and Harris [22] conducted experimental studies to investigate the effect of CFRP strips bonded to bottom flange of notched steel beams under fatigue loading. They also developed a nonlinear FE model that accounts for damage in steel-CFRP interface. It was reported that the

response of the interface under fatigue loading depends on the stress range and the number of fatigue cycles.

Wu et al. [23] studied the effect of fatigue cyclic load on bond behavior between ultrahigh-modulus CFRP composite patch and steel substrate by experimenting double trap joints specimens under fatigue and static loading. Using microscopic examination, a very small localized region of debonding caused by fatigue loading was detected. This observation explained the difference between static load-induced debonding and fatigue load-induced debonding.

Colombi et al. [24] conducted experimental and numerical modeling of CFRP–reinforced single edge–notched tension coupons subjected to fatigue loading. They considered different initial damage levels and patch configurations. An initial semi elliptic-shaped debonding region with length of major axis set equal to crack length and aspect ratio of 1/5 was assumed in numerical model.

Zheng and Dawood [25] focused on the importance of accurately prediction of the shape and size of debonding region on repaired cracked steel structures. They reported that Results indicated that altering the shape and increasing the size of the debonded region could change the calculated crack growth rate by up to 54 times. The results were used to validate the developed numerical FE model. However, developed model focused on mode-I cracks, and also it does not account for fatigue load-induced debonding.

Mohabeddine et al. [26, 27] developed analytical approaches for predicting fatigue life of both-side retrofitted metallic structural details. However, their model does not represent the effect of the debonding of composite patch in an explicit way.

The existence of debonding in the interface of metal and composite in cracked metallic structures that are repaired with adhesively bonded FRP composite patch was acknowledged in reviewed researches. Despite all mentioned efforts to explain the debonding phenomenon, some aspects of the problem are still missing. Up to authors' knowledge, the extent of the effect of debonding around inclined cracks has not been determined. most of previous studies on fracture analysis of FRP-repaired panels were focused on uniaxial loading in mode-I condition. While in the real-life applications, the structures experience general mixed-mode conditions. Hence, an investigation of the effect of debonding on crack geometry in 3-D problems is still missing. Besides, the interaction between crack propagation in metal and damage in adhesive layer has not been discussed. The effect of ductility and strength characteristics of adhesive material on the shape and size of debonding region needs to be investigated.

In light of this premise, the main objective of this study is to deal with the above-mentioned shortcoming in previous studies in the context of crack growth analysis of the repaired panels considering the general mixed-mode fracture conditions with real crack front modeling. A numerical study was established to assess the effect of debonding on the performance of a GFRP-patched aluminum structure with initial crack. In this study, the effect of including or excluding the damage in adhesive layer on the global performance of the patched structure during fatigue loading was investigated. For this purpose, the a-N (length of crack versus number of loading cycles) curves obtained from analyses that include/exclude the damage in adhesive layer were compared for different patching sequences and different adhesives. Additionally, the interaction between crack growth in the plate and damage in adhesive layer was discussed to determine if the debonding of the patch leads to crack growth acceleration in the patched plate or vice versa. Finally, the effect of including debonding in the analysis on the geometry of the crack

obtained from analysis was discussed. This is important in single-side patched structures, due to asymmetric conditions.

A bult-in python script was developed in Abaqus finite element program that accounts for crack growth in the aluminum plate and progressive damage of adhesive during fatigue loading simultaneously. Additionally, in order to invoke the general mixed-mode fracture condition, at which the crack growth is controlled by three components of SIF, a plate with inclined crack was selected. 3D crack geometry was modeled using extended finite element method (XFEM) while the damage in adhesive layer due to static and fatigue loading was accounted for using cohesive zone method (CZM).

The rest of this paper is organized as follows: theoretical basis for modeling of high cycle fatigue crack propagation using XFEM method are presented in section 2. This section elaborates the simulation of fatigue crack growth within the aluminum plate. Section 3 is dedicated to the CZM method that is used for simulation of damage in adhesive layer due to both static and fatigue loadings. The analysis and modeling are the subject of section 4. Finally, the results and discussion are presented in section 5.

2. XFEM-High cycle fatigue model

2.1. Crack modeling using XFEM

S-N curve-based damage mechanics and fracture mechanics are the two main approaches to estimating fatigue life of structural components. S-N curves can be used to predict the fatigue life of non-cracked structures, while fracture mechanics is a more sophisticated approach to fatigue life assessment that takes into account the initial cracks in fatigue life assessment [28].

Modeling of cracks and other discontinuities using finite element method imposes a restraint to the model which is the conformity of the mesh to the geometric discontinuity.

The extended finite element method (XFEM) which is an extension of conventional finite element method is an alternative for conforming mesh of modeling discontinuities [29].

In fracture mechanics context, the enrichment functions typically consist of two distinct groups of functions: the crack-tip asymptotic functions that are responsible for representing singularity around the crack tip, and a jump function that is included to represent the discontinuity across the crack surface. In XFEM, a displacement vector function **u** is approximated in form of partition of unity as:

$$\mathbf{u}(\mathbf{X}) = \mathbf{u}_{FEM}(\mathbf{X}) + \mathbf{u}_{XFEM}(\mathbf{X}) = \sum_{I \in N} N_I(\mathbf{X}) \left[\mathbf{u}_I + \underbrace{H(\mathbf{X})\mathbf{a}_I}_{I \in N_F} + \underbrace{\sum_{\alpha=1}^{4} F_\alpha(\mathbf{X}) b_I^\alpha}_{I \in N_C} \right] \tag{1}$$

Where $(\mathbf{X}) = \{x, y, z\}$ denotes the three-dimensional coordinate system; $N_I(\mathbf{X})$ is the conventional set of nodal shape functions; the first term of the right-hand side of the equation,

$\mathbf{u}_I$, is the usual nodal vector of displacements associated with un-cracked elements; the second term is the product of jump function, $H(\mathbf{X})$, and crack face enriched degrees of freedom vector, $\mathbf{a}_I$, across the crack face; and the third term, representing the asymptotic enrichment in crack tip elements, is the product of enrichment functions, $F_\alpha(\mathbf{X})$, and associated enriched degrees of freedom, b_I^α. This should be noted that enrichment procedure in XFEM is node-wise; rather than element-wise. The first term on the right-hand side of equation (1) is applicable to all the nodes included in the analysis (N); the second term is used for the nodes in the support zone in which their shape function is cut by crack boundaries (N_F); and the third one is valid for crack tip nodes which are located in the support zone of their shape functions (N_C). As by omitting the second and third terms of equation (1), the conventional FEM formulation can be obtained.

The jump function across the crack face is a Heaviside function, expressed as:

$$H(\mathbf{X}) = \begin{cases} 1, & (\mathbf{X}-\mathbf{X}^*).\mathbf{n} \geq 0 \\ -1, & otherwise \end{cases} \quad (2)$$

In which, $\mathbf{X}$ is a Gauss point, $\mathbf{X}^*$ is a point on the crack surface with minimum distance to $\mathbf{X}$, and $\mathbf{n}$ is the unit normal vector of crack surface at $\mathbf{X}^*$ [30].

Asymptotic crack tip functions, on the other hand, are expressed in polar (r, θ) coordinate system whose origin is located at the crack tip. For an isotropic material, these functions take the form of:

$$F_\alpha(\mathbf{X}) = \left[\sqrt{r}\sin\frac{\theta}{2}, \sqrt{r}\cos\frac{\theta}{2}, \sqrt{r}\sin\theta\sin\frac{\theta}{2}, \sqrt{r}\sin\theta\cos\frac{\theta}{2} \right] \quad (3)$$

In which, r denotes radial distance from sampling Gauss point to the crack tip (origin of the coordinate system).

It is clear from equations (1) and (3), by including crack tip enrichment functions in displacement field approximation can model the singularity of stress at crack tip by keeping track of crack tip location as the crack propagates. This is as cumbersome as updating the mesh in conventional finite element analysis of propagating crack. Therefore, in commercial finite element programs such as ABAQUS, crack tip enrichment is used only in analysis of stationary cracks, which is carried out in order to calculate stress intensity factors in a cracked structure [30, 31]. It was required to develop a Python script code in order to be able to use the crack-tip enrichment in ABAQUS. The scripting method will be discussed in section 2.3.

The geometry of non-smooth moving crack is defined using the Level Set Method (LSM). In 3D space, two orthogonal signed distance functions ϕ and φ are defined, where the intersection of them denote the crack front. $\phi(\mathbf{X},t)$ represent the distance of point $\mathbf{X}$, at time t from the crack surface. While the distance between the point under consideration and orthogonal surface at crack face is designated by $\varphi(\mathbf{X},t)$.

2.2. Fatigue crack growth model

Crack growth rate due to fatigue loading (*da/dN*) is often related to Stress Intensity Factor (SIF) using power function equations. These equations are obtained from fitting mathematical expressions to experimental data. Paris law expression is a well-known relation for crack growth under constant amplitude fatigue loading. This expression uses two material constants as follows:

$$\frac{da}{dN} = c(\Delta K)^m \tag{4}$$

where $\frac{da}{dN}$ is crack growth rate, a is the crack length, N is the number of load cycles, c and m are material constants, and ΔK is stress intensity factor range in a loading cycle.
In general mixed-mode crack problems, like in the case of inclined cracks, the crack grows due to three SIFs (K-I, K-II, K-III that represent Mode-I, Mode-II, and Mode-III of fracture). For this reason, in order to calculate the crack growth rate, an equivalent stress intensity factor is required to be used in equation (4). In this regard, Richard [32] equation which has been shown that yields acceptable results [19] was used. Besides this criterion gives an equation for crack deflection angles. This equation proposes an equivalent stress intensity factor as follows:

$$K_{eq} = \frac{K_I}{2} + \frac{1}{2}\sqrt{K_I^2 + 4(\alpha_1 K_{II})^2 + 4(\alpha_2 K_{III})^2} \tag{5}$$

where $\alpha_1 = \frac{K_{IC}}{K_{IIC}}$ and $\alpha_2 = \frac{K_{IC}}{K_{IIIC}}$. Values of $\alpha_1 = 1.155$ and $\alpha_2 = 1$ were recommended.
According to this criterion, unstable crack growth occurs when $K_{eq} \geq K_{IC}$.

2.3. High cycle fatigue XFEM script

ABAQUS uses phantom node method which is a modified version of XFEM for modeling propagating cracks. In this method, crack-tip enrichment is excluded (Setting $F_\alpha(\mathbf{X}) = 0$) and only Heaviside crack face enrichment is considered [16, 30, 31]. Stationary cracks, on the other hand, are modeled using standard XFEM, which will be discussed in section 3.1. A Python script code was developed in this study to carryout high cycle fatigue analysis using XFEM with crack-tip enrichment in ABAQUS.

ABAQUS uses interaction integral method [33] to calculate stress intensity factors in crack front for stationary crack problems. After completion of the analysis, the script extract needed data from the analysis to define the new crack geometry for a limited number of cycles passed. This loop is repeated until the critical intensity factor at the occurrence of catastrophic failure is reached.

The following tasks are carried out by the provided computer script code to model the fatigue crack growth using XFEM:

1. Produce the geometry, material properties, and sections of the problem except the crack.
2. Generate the mesh assembly with sufficient refinement and assign mesh to the geometry.

3. Allocate loads and boundary conditions to the problem.
4. Define the geometry of the crack based on previous step data.
5. Submit a quasi-static stationary crack XFEM analysis.
6. Extract the required data from interaction integral analysis performed by ABAQUS.
7. Calculate the equivalent stress intensity factor based on equation (5).
8. Determine the crack growth rate based on equation (4).
9. Define new crack geometry.
10. Repeat steps 4 to 9, until reaching a predefined critical crack length, or equivalent critical stress intensity factor.
Finally, the number of cycles of different steps are summed up to calculate the fatigue life of the specimen. A flowchart of high cycle fatigue XFEM script developed in this study, is given in Figure 1.

3. Method of CZM for the defined problem

3.1. Constitutive equation

The kinematics of cohesive elements include only three components of nominal tractions: one normal traction in thickness direction, t_n, and two in-plane tangential shear traction components, t_s and t_t. The nominal traction is defined as corresponding force magnitude divided by the original area at a material point. Denoting the nominal and two in-plane tangential opening components, δ_n, δ_s, δ_t, respectively, the strain components are defined as:

$$\varepsilon_n = \frac{\delta_n}{h_0}, \quad \varepsilon_s = \frac{\delta_s}{h_0}, \quad \varepsilon_t = \frac{\delta_t}{h_0} \tag{6}$$

Where h_0 is initial thickness of the element.

The linear elastic behavior in the CZM can then be expressed in the form of an elastic constitutive matrix relating the nominal tractions and strains in tension and shear as follows:

$$\mathbf{t} = \begin{Bmatrix} t_n \\ t_s \\ t_t \end{Bmatrix} = \begin{bmatrix} k_{nn} & k_{ns} & k_{nt} \\ k_{sn} & k_{ss} & k_{st} \\ k_{tn} & k_{ts} & k_{tt} \end{bmatrix} \begin{Bmatrix} \varepsilon_n \\ \varepsilon_s \\ \varepsilon_t \end{Bmatrix} = \mathbf{K}\varepsilon \tag{7}$$

The stiffness matrix, $\mathbf{K}$ represents the adhesive material properties. For thin adhesive layers, an adequate approximation is achieved, setting [34]:

$$k_{nn} = E, \quad k_{ss} = k_{tt} = G, \quad k_{ij} = 0, \quad i, j = n, s \tag{8}$$

Where E and G are the moduli of elasticity in normal and tangential directions, respectively.

3.2. Static and Fatigue Damage

In a traction-separation model, the material is assumed to behave linearly until a critical limit reached. This point, which is defined by a damage initiation criterion, is a trigger point for damage evolution. Afterwards, as the load increases the damage progresses based on a damage evolution criterion and results in stiffness degradation. This phase continues until the material is fully damaged.

The maximum nominal stress criterion assumes damage initiation as one of stress components reaches its critical limit. On the other hand, the quadratic nominal stress criterion investigates a quadratic combination of stresses to check damage initiation. The quadratic nominal stress criterion is expressed in the form of:

$$\frac{\langle t_n \rangle}{t_n^0} + \frac{t_s}{t_s^0} + \frac{t_t}{t_t^0} = 1 \qquad (9)$$

Where $\varepsilon_i^0,\quad t_i^0,\quad i = n,s,t$ are critical nominal stresses in normal and shear directions. The symbol $\langle . \rangle$ is Macaulay bracket that is used to denote that compressive stress does not initiate damage [35].

Once the damage initiation limit is met, the damage growth is incorporated by starting stiffness degradation. The rate of damage is described based on a damage evolution criterion. Overall damage in the material is determined with a damage variable, a scalar usually indicated by D, which represents the effect of all mechanisms that may lead to material degradation. The damage variable, D, grows monotonically from 0 to 1 as load increases. The effect of stiffness degradation that is represented by D, is reflected within global solution of the analysis via:

$$\begin{aligned} t_n &= \begin{cases} (1-D)\bar{t}_n, & \bar{t}_n \geq 0 \\ \bar{t}_n, & otherwise \end{cases} \\ t_s &= (1-D)\bar{t}_s \\ t_t &= (1-D)\bar{t}_t \end{aligned} \qquad (10)$$

Where $\bar{t}_i, i = n,s,t$ are traction components assuming linear elastic behavior for corresponding nominal strains.

The mixed mode traction-separation response is a combination of its response in pure modes. B-K [36] fracture criterion provides a well-known relation for critical fracture energy in mixed mode. For isotropic fracture with $G_{II} = G_{III}$:

$$G^C = G_I^C + (G_{II}^C + G_I^C)\left(\frac{2G_{II}}{2G_{II} + G_I}\right)^{\eta} \qquad (11)$$

An efficient and straightforward way to predict the strength of adhesively bonded joints under fatigue loading without any requirement on joint configuration was proposed in [21].

This method that accounts for the deleterious effect of fatigue loading within CZM framework, uses a bilinear traction-separation response to represent the behavior of the adhesive with no fatigue loading. The traction-separation response of CZM is then degraded in material points that reach a principal nominal strain limit. The damage resulted from fatigue loading is given by:

$$\frac{\Delta D_F}{\Delta N} = \begin{cases} \alpha(\varepsilon_{\max} - \varepsilon_{th})^{\beta}, & \varepsilon_{\max} \geq \varepsilon_{th} \\ 0, & otherwise \end{cases}$$
$$\varepsilon_{\max} = (\frac{\varepsilon_{th}}{2}) + \sqrt{(\frac{\varepsilon_n}{2})^2 + (\frac{\varepsilon_s}{2})^2 + (\frac{\varepsilon_t}{2})^2} \qquad (12)$$

Where $\varepsilon_{\max}$ is the maximum principal nominal strain in a cycle, and $\alpha, \beta, \varepsilon_{th}$ are material constants, to be calibrated through experimental tests.

The traction-separation response is a function of the fatigue damage index D_F. By increasing from 0 to 1, D_F degrades the strength and energy limits that could be tolerated by the material. This effect is reflected in static damage variable, D_S, which eventually results in stiffness degradation and removing fully damaged elements from analysis.

4. Modeling and analysis

4.1. Problem description

In order to accomplish the aims of the study, a 3-D problem with existing experimental results was selected. The problem was previously carried out by Hosseini-Tudeshkey et al. [37]. The geometry of the problem parts, loading and boundary conditions are schematically shown in Figure 2.

Table 1 summarizes the geometrical and initial conditions of the problem.

Mechanical constants of the aluminum alloy 2024-T3 and glass/epoxy composite patch are listed in Table 2 and Table 3, respectively.

The crack propagation was assumed to be limited to bulk material of aluminum plate, and will never extends within adhesive and composite patch. Therefore, Paris law constants are needed for this material. Table 4 presents these parameters for fatigue crack growth in aluminum alloy 2024-T3.

Three epoxy adhesives were considered in this study. The adhesive Araldite AV138 was used to represent high strength brittle adhesives. Araldite 2015, on the other hand stands for ductile adhesive, but less ultimate strength. This adhesive tolerates large plastic flow prior to failure. The third one is FM 73 OST adhesive. This adhesive benefits from both high strength and ductility.

4.2. Numerical model

The problem was modeled and analyzed using developed Python script code in which a 3-D model was developed and well-suited in finite element numerical simulations for each loading cycle. Extended finite element method (XFEM) with crack face and asymptotic crack-tip enrichment was used to model crack propagation due to fatigue loading in the analysis.

ABAQUS was also linked to FORTRAN compiler through Visual studio program to enable user-defined subroutines incorporation within finite element analysis.

A View of 3D model with different parts is presented in Figure 3-a. While in Figure 3-b a magnified view of the refined mesh around the initial crack is shown. The blue-colored zone indicates the XFEM-enriched region, at which the crack in the aluminum plate would propagate.

The aluminum plate and composite patch were modeled using C3D8 hexahedron solid elements. These elements are consisted of 8 nodes, and full integration method is used in stress field calculation of them. COH3D8 hexahedron cohesive element which are compatible with brick elements were used for adhesive layer simulation. The problem was simulated using 87,604 solid elements and 110,624 nodes. The geometry of the problem was meshed with sufficiently small size around 0.25 mm at the vicinity of crack tip and in the crack growth direction which are the most susceptible zones for adhesive damage.

A constant amplitude load was applied to the structure. The load in a fatigue step ramps up from its minimum level ($0.1\sigma_0$) in the beginning of the step to its highest level (σ_0) in the mid-time of the step. Then the load is decreased again to its lowest level, in the end of the step. However, the load remains positive even in its lowest level. Thus, the problem is classified as tension-tension fatigue loading problem. Fatigue crack growth was simulated using a 3D model.

Adhesive layer was modeled using cohesive zone method (CZM), considering static and fatigue damage. In order to implement this method in finite element model, a user-defined subroutine USDFLD was developed in FORTRAN and incorporated within ABAQUS model. CZM constants and damage parameters of adhesive are presented in Table 5.

The damage propagation due to fatigue loading was calculated using the method proposed in [21]. The material constants used for adhesive materials in this study are presented in Table 6.

5. Results and discussion

5.1. Model verification

In this section, target points of the study are precisely defined and the results are presented in details. The results obtained from developed numerical model are verified against experimental data, available in the literature. For this purpose, the crack length versus number of fatigue loading cycles (a-N) curves for unpatched plate and patched plate with $[-75]_4$ glass-epoxy composite patch and FM 73 adhesive is analyzed. The analysis was carried out up to the crack length of approximately 16 mm in X direction which was considered as critical crack length for Paris law crack growth.

Figure 4 illustrates a comparison between numerical results obtained from the current work and the experimental measurements available in [37] up to crack length of 16 mm in X direction.

It is seen acceptable agreement between the numerical and experimental curves. The same comparison between the crack growth behavior (a-N curve) of the patched plate with $[-75]_4$ lay-up patch and FM 73 adhesive predicted by this study against Experimental work in [37] is presented. Satisfactory agreement between the numerical results of CZM damage model and reference experimental results is observed.
This shall be noted that omitting the effect of damage in adhesive layer by [37] led to a considerable eccentricity in numerical results from experimental ones in their study. This observation verifies the more accuracy of considering CZM approach for capturing the effect of damage in adhesives of composite patched structures subjected to fatigue load with respect to the previous studies which neglected the damage in adhesive layer.

5.2. Fatigue life prediction

In this study, the progressive damage in adhesive layer was modeled using cohesive zone model (CZM). This method was formulated for fatigue and static damage, simultaneously, as the main contribution of the current investigation. The limits for static damage initiation and propagation are determined based on the nominal stress and accumulated strain energy. Fatigue damage, on the other hand, is formulated in a strain basis [21].

The effect of considering damage in adhesive layer (debonding) in the analysis on fatigue life of patched structure is investigated. Three types of adhesive materials and five patch lay-up sequences were considered.

Figure 5 summarizes fatigue life prediction of the plate obtained from numerical models for different patch sequences up to crack length of 16 mm in X direction. The difference of fatigue life predicted by no-damage model in which the damage in adhesive layer was neglected, with respect to CZM model is given in parenthesis.

Figure 5 shows that by implementing CZM damage behavior in the numerical analysis, the fatigue life prediction of the structure was reduced with respect to the case without cohesive damage considerations. The difference between results of models with and without CZM damage in adhesive layer was obtained in a range of 8.4 to 23.2 percent. The results show less sensitivity to the patch lay-up configurations and more sensitivity to adhesive material. FM 73 adhesive that benefits from high strength and ductility, show the best performance over other adhesives. Meanwhile, using AV138 and 2015 adhesives results in more reduction of fatigue life that indicates both ultimate strength and plastic deformation prior to failure are important in adhesive performance in fatigue loading.

It is also observed that the composite patch considerably increases the life cycle of the metal plate by a minimum ratio of 100 percent. The patch lay-up configurations of $[0]_4$, $[45]_4$ and $[-45]_4$ show less effect on fatigue life improvement in comparison with $[90]_4$ and $[-75]_4$. As can be seen, the latter patch lay-up arrangements increase the fatigue life cycle more than 200 percent with respect to un-patched ones. It is feasible that the effect of the patch is maximized when the

composite patch fiber directions are placed in perpendicular direction with respect to crack growth direction.

5.3. Crack growth – adhesive damage interaction

An important aspect of investigating the effect of debonding on performance of repairing patch is the interaction of damage in adhesive (debonding) with crack growth in bulk material. Knowing this fact that damage of adhesive layer has led to crack growth intensification in bulk material or vice versa, if damage in adhesive has been majorly caused by crack growth helps in achieving more reasonable design. For this purpose, crack length on patched and un-patched surfaces versus number of loading cycles (a-N curves) obtained from models that account for damage of adhesive and those that do not account for that are reviewed. These curves shall be considered in coincident with damage evolution in adhesive layer.

Figures 6 -9 show a-N curves for patched plate with $[-75]_4$ and $[90]_4$ lay-up patches and FM 73 adhesive, followed by damage evolution in adhesive layer for this specimen, respectively.

Considering Figures 6 and 8, it is observed that a-N curve for both patched and un-patched surfaces of damage-including model keep the same pattern of that of no-damage model. This means that debonding (if exists) is dominated by fatigue crack growth in considered specimens. Figures 7 and 9 verify this conclusion. It is observed from the later figures that the crack reaches a specific point in bulk material prior to damage initiation in adjacent adhesive point.

Figures 10 -13 show a-N curves for patched plate with $[-75]_4$ and $[90]_4$ lay-up patches and AV138 adhesive, followed by damage evolution in adhesive layer for this specimen, respectively.

Figures 10 and 12, show noticeable increase in curvature and decrease in length of a-N curves for both patched and un-patched surfaces of damage-including models with respect to that of no-damage model. Large distance between the curves, and changed pattern of damage-including model's curves demonstrate the impact of debonding. Figures 11 and 13 show noticeable area of debonding evolution that explain noticed difference in a-N curves. However, Figures 11 and 13 show that the length of debonding area remains smaller than crack length on patched surface. It could be concluded from this observation that damage in adhesive is leaded by crack growth in bulk material in specimens with AV138, too.

Figures 14 -17 show a-N curves for patched plate with $[-75]_4$ and $[90]_4$ lay-up patches and AV138 adhesive, followed by damage evolution in adhesive layer for this specimen, respectively.

Figures 14 and 16, also show significant increase in curvature and decrease in length of a-N curves for both patched and un-patched surfaces of damage-including models with respect to that of no-damage model. The difference is more sensible on patched surface. The impact of debonding on a-N curve is noticeable. Figures 15 and 17 show visible area of debonding evolution that explain noticed difference in a-N curves. These figures show that in final stages, the length of damaged zone is greater than the length of crack on patched surface. This means that debonding occurs in a specific point of adhesive prior to cracking of adjacent bulk point, in

final loading cycles. It could be argued that in this stage, the crack growth in bulk material is leaded by debonding.
As a concluding remark for this section, it may be expressed that for specimens with FM 73 and AV138 adhesives, global response of patched structure is dominated by crack growth in bulk material. Meanwhile, for specimens with 2015 adhesive, an interaction between crack growth in bulk material and damage in adhesive material (debonding) may be observed.

5.4. Crack geometry

By considering the adhesive damage in the analysis and examining the CZM configuration on the crack geometry, the crack development path was investigated in this part. For brevity concerns, only the models with $[-75]_4$ lay-up sequence and FM73 adhesive has been studied for this purpose. Crack geometry over loading cycles obtained from the model that do not include the damage in the adhesive layer and the model that include the damage in the adhesive layer are presented in Figure 18 and Figure 19, respectively.

Comparing the geometry of crack in Figures 18 and 19, it is obvious that including the damage in adhesive layer results in smooth crack geometry. For better explanation, the projection of the crack on different planes is shown in next figures.

The projection of crack trajectories on the metal surface of the patched plate with $[-75]_4$ patch lay-ups in XY plane are shown in Figure 20.

The curves of crack trajectories have a mild positive slope during crack development in both models. However, including damage in analysis results in smoother curve.
Another contribution of the current study is considering the influence of damage in adhesive layer on crack development geometry by means of crack front shape in both XZ and YZ planes. Figures 21 and 22 show the calculated crack front shape in XZ and YZ planes obtained from numerical model for no-damage and damage-including models, respectively.

In Figures 21-22 (a), a regular pattern for crack front growth in XZ plane is observed. It is obvious that the crack grows non-uniformly along the thickness of the plate. The trend of crack front in this plane, varies from an approximately straight line to inclined curves with high curvature, as crack grows. The non-linearity trend of crack front shape is maximized at patched surface, and minimized at un-patched one. This behavior is caused by the asymmetry conditions of the patched plate which results in out of plane bending.

Comparing part (a) of Figures 21-22, it is seen that considering damage in adhesive layer affect the obtained crack front curve in XZ plane, significantly. Including the damage of adhesive layer leads to reduction in stiffness of the patched plate, and therefore the resulted out of plane bending moment. Eventually, the crack grows smoothly which indicate that the effect of patching is reduced as the damage in adhesive develops.

On the other hand, the shape of crack fronts in YZ plane as depicted in Figures 21-22 (b) show less sensitivity to including of damage in the analysis. In YZ plane, crack development

starts with an approximately straight line. By increasing the fatigue cycle numbers, the trend of crack front obliged to nonlinear with an extremum point near patched surface. The curvature of crack front curve in this plane reverses in final stages of crack growth. The difference between the curves of Figure 21 with those of Figures 22 is the point of curvature reversal that occur in an earlier number of cycles in Figures 22.

5- Conclusions

Simultaneus modeling of fatigue crack growth and damage of adhesive layer in a composite-patched aluminum plate with inclined crack was investigated thoroughly. A Python script code was developed in this study to automate fatigue crack propagation in the metal plate, using standard XFEM in ABAQUS. The damage in the adhesive layer was modeled using CZM to investigate the efficiency of this method for capturing behavior of adhesive in composite-patched cracked plate subjected to fatigue loading in general mixed mode of fracture. A user-defined USDFLD subroutine was developed to account for the effect of fatigue cyclic loading on adhesive material. Three types of adhesives were used in this study. Brittle high failure strength, ductile low failure strength and ductile high failure strength adhesives were considered.

It was concluded that neglecting damage of adhesive layer (debonding) from analysis results in 8.4 to 23.2 percent overestimated fatigue life. As an engineering application conclusion, this research show that specimens with high ductility and high failure strength (FM 73 OST epoxy adhesive) experience less damage in problem under consideration. Meanwhile adhesives with less failure strength or ductility experienced more damage.

Studying the interaction between crack growth in bulk material and damage in adhesive layer showed that the global response of studied structures is dominated by crack growth in metal. However, in specimens with low failure strength adhesive, an interaction between crack growth in bulk material and damage in adhesive layer was noticed.

The investigation of the geometry of crack for repired plates with $[-75]_4$ lay-up patch, revealed the significant impact of including damage in adhesive layer on crack front development shape. Smoother crack geometry was obtained from damage-including models.

This research my be extended for variable-amplitude fatigue loading in a future work.

Refferences

[1] Maleki, A., Saeedifar, M., Najafabadi, et al. "The fatigue failure study of repaired aluminum plates by composite patches using acoustic mission", *Engineering Fracture Mechanics*, *210*, pp. 300-311(2019). DOI: 10.1016/j.engfracmech.2017.12.034

[2] Philip, R. E., Andrushia, A. D., Nammalvar, A., et al. "A Comparative Study on Crack Detection in Concrete Walls Using Transfer Learning Techniques", *Journal of Composites Science*, *7*(4), 169 (2023). DOI: 10.3390/jcs7040169

[3] Roy, K., Lim, J. B., Yousefi, et al. "Low fatigue response of crest-fixed cold-formed steel drape curved roof claddings.", *International Specialty Conference on Cold-Formed Steel Structures* (2018), 4, https://scholarsmine.mst.edu/isccss/24iccfss/session10/4.

[4] Baker, A. A., Rose, L. F., & Jones, R. (Eds.). "Advances in the bonded composite repair of metallic aircraft structure", Elsevier (2003). eBook ISBN: 9780080522951

[5] Bellali, M. A., Serier, B., Mokhtari, M., et al. "XFEM and CZM modeling to predict the repair damage by composite patch of aircraft structures: Debonding parameters", *Composite Structures*, *266*, pp. 113805(2021). DOI: 10.1016/j.compstruct.2021.113805

[6] Mohammed, S. M. K., Mhamdia, R., Albedah, A., et al. "Fatigue crack growth in aluminum plates repaired with different shapes of single-sided composite patches." *International Journal of Adhesion and Adhesives*, *105*, pp. 102781(2021). DOI: 10.1016/j.ijadhadh.2020.102781

[7] Zarrinzadeh, H., Kabir, M. Z., & Deylami, A. "Extended finite element fracture analysis of a cracked isotropic shell repaired by composite patch." *Fatigue & Fracture of Engineering Materials & Structures*, *39*(11), pp. 1352-1365(2016). DOI: 10.1111/ffe.12446

[8] Ke, L., Li, C., He, J., et al. "Enhancing fatigue performance of damaged metallic structures by bonded CFRP patches considering temperature effects." *Materials & Design*, *192*, pp. 108731(2020). DOI: 10.1016/j.matdes.2020.108731

[9] Hosseini, A. S., Zavvar, E., & Ahmadi, H. "Stress concentration factors in FRP-strengthened steel tubular KT-joints.", *Applied Ocean Research*, *108*, 102525(2021). DOI: https://doi.org/10.1016/j.apor.2021.102525

[10] Ke, L., Zhu, F., Chen, Z., et al. "Fatigue failure mechanisms and probabilistic SN curves for CFRP–steel adhesively bonded joints." *International Journal of Fatigue*, *168*, pp. 107470 (2023). DOI: 10.1016/j.ijfatigue.2022.107470

[11] Baghdadi, M., Serier, B., Salem, et al. "Modeling of a cracked and repaired Al 2024T3 aircraft plate: effect of the composite patch shape on the repair performance: Effect of the composite patch shape on the repair performance.", *Frattura ed Integrità Strutturale*, *13*(50), pp. 68-85(2019). DOI: 10.3221/IGF-ESIS.50.08

[12] Albedah, A., Mohammed, S. M. K., Bouiadjra, B. B., et al. “Effect of the patch length on the effectiveness of one-sided bonded composite repair for aluminum plates.”, *International Journal of Adhesion and Adhesives*, *81*, pp.83-89(2018). DOI: 10.1016/j.ijadhadh.2017.11.012

[13] Orsatelli, J. B., Paroissien, E., Lachaud, F., et al. “Bonded flush repairs for aerospace composite structures: a review on modelling strategies and application to repairs optimization, reliability and durability.”, *Composite Structures*, pp. 116338(2022). DOI: 10.1016/j.compstruct.2022.116338

[14] Ramalho, L. D., Campilho, R. D., Belinha, et al. “Static strength prediction of adhesive joints: A review.”, *International Journal of Adhesion and Adhesives*, *96*, pp. 102451(2020). DOI: 10.1016/j.ijadhadh.2019.102451

[15] Zarrinzadeh, H., Kabir, M. Z., & Deylami, A. “Experimental and numerical fatigue crack growth of an aluminium pipe repaired by composite patch.”, *Engineering Structures*, *133*, pp.24-32(2017). DOI: 10.1016/j.engstruct.2016.12.011

[16] Zarrinzadeh, H., Kabir, M. Z., & Deylami, A. “Crack growth and debonding analysis of an aluminum pipe repaired by composite patch under fatigue loading.”, *Thin-Walled Structures*, *112*, pp.140-148(2017). DOI: 10.1016/j.tws.2016.12.023

[17] Colombi, P., Bassetti, A., & Nussbaumer, A. “Crack growth induced delamination on steel members reinforced by prestressed composite patch.” *Fatigue & Fracture of Engineering Materials & Structures*, *26*(5), pp. 429-438(2003). DOI: 10.1046/j.1460-2695.2003.00642.x

[18] Sabelkin, V., Mall, S., & Avram, J. B. “Fatigue crack growth analysis of stiffened cracked panel repaired with bonded composite patch.”, *Engineering Fracture Mechanics*, *73*(11), pp. 1553-1567(2006). DOI: 10.1016/j.engfracmech.2006.01.029

[19] Hosseini-Toudeshky, H., Saber, M., & Mohammadi, B. “Finite element crack propagation of adhesively bonded repaired panels in general mixed-mode conditions.” *Finite Elements in Analysis and Design*, *45*(2), pp. 94-103(2009). DOI: 10.1016/j.finel.2008.07.010

[20] Huawen, Y., König, C., Ummenhofer, T., et al. “Fatigue performance of tension steel plates strengthened with prestressed CFRP laminates.” *Journal of Composites for Construction*, *14*(5), pp. 609-615(2010). DOI: 10.1061/%28ASCE%29CC.1943-5614.0000111

[21] Khoramishad, H., Crocombe, A. D., Katnam, K. B., et al. “Predicting fatigue damage in adhesively bonded joints using a cohesive zone model.” *International Journal of fatigue*, *32*(7), pp. 1146-1158(2010). DOI: 10.1016/j.ijfatigue.2009.12.013

[22] Kim, Y. J., & Harries, K. A. “Fatigue behavior of damaged steel beams repaired with CFRP strips.” *Engineering Structures*, *33*(5), pp. 1491-1502(2010).

DOI: 10.1016/j.engstruct.2011.01.019

[23] Wu, C., Zhao, X. L., Chiu, et al. “Effect of fatigue loading on the bond behaviour between UHM CFRP plates and steel plates.”, *Composites Part B: Engineering*, *50*, pp. 344-353(2013). DOI: 10.1016/j.compositesb.2013.02.040

[24] Colombi, P., Fava, G., & Sonzogni, L. “Fatigue crack growth in CFRP-strengthened steel plates.”, *Composites Part B: Engineering*, *72*, pp. 87-96(2015). DOI: 10.1016/j.compositesb.2014.11.036

[25] Zheng, B., & Dawood, M. “Debonding of carbon fiber–reinforced polymer patches from cracked steel elements under fatigue loading.”, *Journal of Composites for Construction*, *20*(6), pp. 04016038(2016). DOI: 10.1061/%28ASCE%29CC.1943-5614.0000694

[26] Mohabeddine, A., Correia, J. A., Montenegro, P. A., et al. “Fatigue crack growth modelling for cracked small-scale structural details repaired with CFRP.”, *Thin-Walled Structures*, *161*, pp. 107525(2021). DOI: 10.1016/j.tws.2021.107525

[27] Mohabeddine, A., Correia, J., Montenegro, P. A., et al. “An approach for predicting fatigue life of CFRP retrofitted metallic structural details.”, *International Journal of Fatigue*, *154*, pp. 106557(2022). DOI: 10.1016/j.ijfatigue.2021.106557

[28] Kakaie, A., Guedes Soares, C., Ariffin, A. K., et al. “Fatigue Reliability Analysis of Submarine Pipelines Using the Bayesian Approach.”, *Journal of Marine Science and Engineering*, *11*(3), pp. 580(2023). DOI: 10.3390/jmse11030580

[29] Xin, H., Liu, J., Correia, J. A., et al. “Mixed-mode fatigue crack propagation simulation by means of Geq and Walker models of the structural steel S355.”, *Theoretical and Applied Fracture Mechanics*, pp. 103717(2023). DOI: 10.1016/j.tafmec.2022.103717

[30] Dassault Systèmes. Simulia User Assistance 2020, ABAQUS. https://www.3ds.com/products/simulia

[31] Xin, H., Correia, J. A., & Veljkovic, M. “Three-dimensional fatigue crack propagation simulation using extended finite element methods for steel grades S355 and S690 considering mean stress effects.”, *Engineering Structures*, *227*, pp. 111414(2021). DOI: 10.1016/j.engstruct.2020.111414

[32] Richard, H. A., Buchholz, F. G., Kullmer, G., et al. “2D-and 3D-mixed mode fracture criteria.”, *Key Engineering Materials* 251, pp. 251-260(2003). DOI: 10.4028/www.scientific.net/KEM.251-252.251

[33] Singh, I. V., Mishra, B. K., Bhattacharya, S., et al. “The numerical simulation of fatigue crack growth using extended finite element method.” *International Journal of Fatigue*, *36*(1), pp. 109-119(2012). DOI: 10.1016/j.ijfatigue.2011.08.010

[34] Campilho, R. D., Banea, M. D., Neto, J. A. B. P., et al. “Modelling adhesive joints with cohesive zone models: effect of the cohesive law shape of the adhesive layer.”, *International journal of adhesion and adhesives*, *44*, pp. 48-56(2013).
DOI: 10.1016/j.ijadhadh.2013.02.006

[35] Hu, P., Shi, Z. W., Wang, X. X., et al. “Strength degradation of adhesively bonded single-lap joints in a cyclic-temperature environment using a cohesive zone model.”, *The Journal of Adhesion*, *91*(8), pp. 587-603(2015). DOI: 10.1080/00218464.2014.915754

[36] Benzeggagh, M. L., & Kenane, M. J. C. S. (1996). “Measurement of mixed-mode delamination fracture toughness of unidirectional glass/epoxy composites with mixed-mode bending apparatus.”, *Composites science and technology*, *56*(4), 439-449(1996).
DOI: 10.1016/0266-3538(96)00005-X

[37] Hosseini-Toudeshky, H., & Mohammadi, B. “Mixed-mode numerical and experimental fatigue crack growth analyses of thick aluminium plates repaired with composite patches.”, *Composite Structures*, *91*(1), pp. 1-8(2009).
DOI: 10.1016/j.compstruct.2009.04.022

Tables

Table 1- Geometrical parameters and initial conditions of the problem.

Parameter	Definition	Magnitude	
σ_0	Fatigue Load	110	MPa
W	Plate Width	48	mm
L	Plate Length	170	mm
t	Plate thickness	2.29	mm
Wp	Patch Width	48	mm
Lp	Patch Length	100	mm
tp	Patch thickness	0.72	mm
ta	Adhesive thickness	0.1	mm
2a	Initial crack length	10	mm
α	Initial crack direction	45°	
θ	Fiber Angle	Var.	

Table 2- Mechanical properties of aluminum alloy 2024-T3 [37].

Elasticity modulus GPa)	Poisson's ratio
71.02	0.3

Table 3- Mechanical properties of glass/epoxy composite patch [37].

Elasticity modulus GPa)		Shear modulus (GPa)		Poisson's ratio	
E_{11}	27.82	G_{12}	2.56	ν_{12}	0.31
E_{22}	5.83	G_{13}	2.56	ν_{13}	0.31
E_{33}	5.83	G_{23}	2.24	ν_{23}	0.41

Table 4- Paris's law constants for aluminum alloy 2024-T3 [37].

C	m
2.29 e-14	3.7927

Table 5- CZM parameters for adhesive materials [34, 37].

Parameter		FM 73 OST (FM 73)	Araldite AV138 (AV138)	Araldite 2015 (2015)
E	(MPa)	1830	4890	1850
G	(MPa)	668	1560	560
T_I	(MPa)	114	39.45	21.63
T_{II}	(MPa)	66	30.2	17.9
G_I	(N/mm)	1.4	0.2	0.43
G_{II}	(N/mm)	2.8	0.38	4.70
η	(B-K law)	2	2	2

Table 6- Fatigue damage parameters of adhesive materials.

Parameter	FM 73 OST	Araldite AV138	Araldite 2015
α	1.5	1.5	1.5
β	2	2	2
ε_{th}	0.0319	0.0035	0.0167

Figures

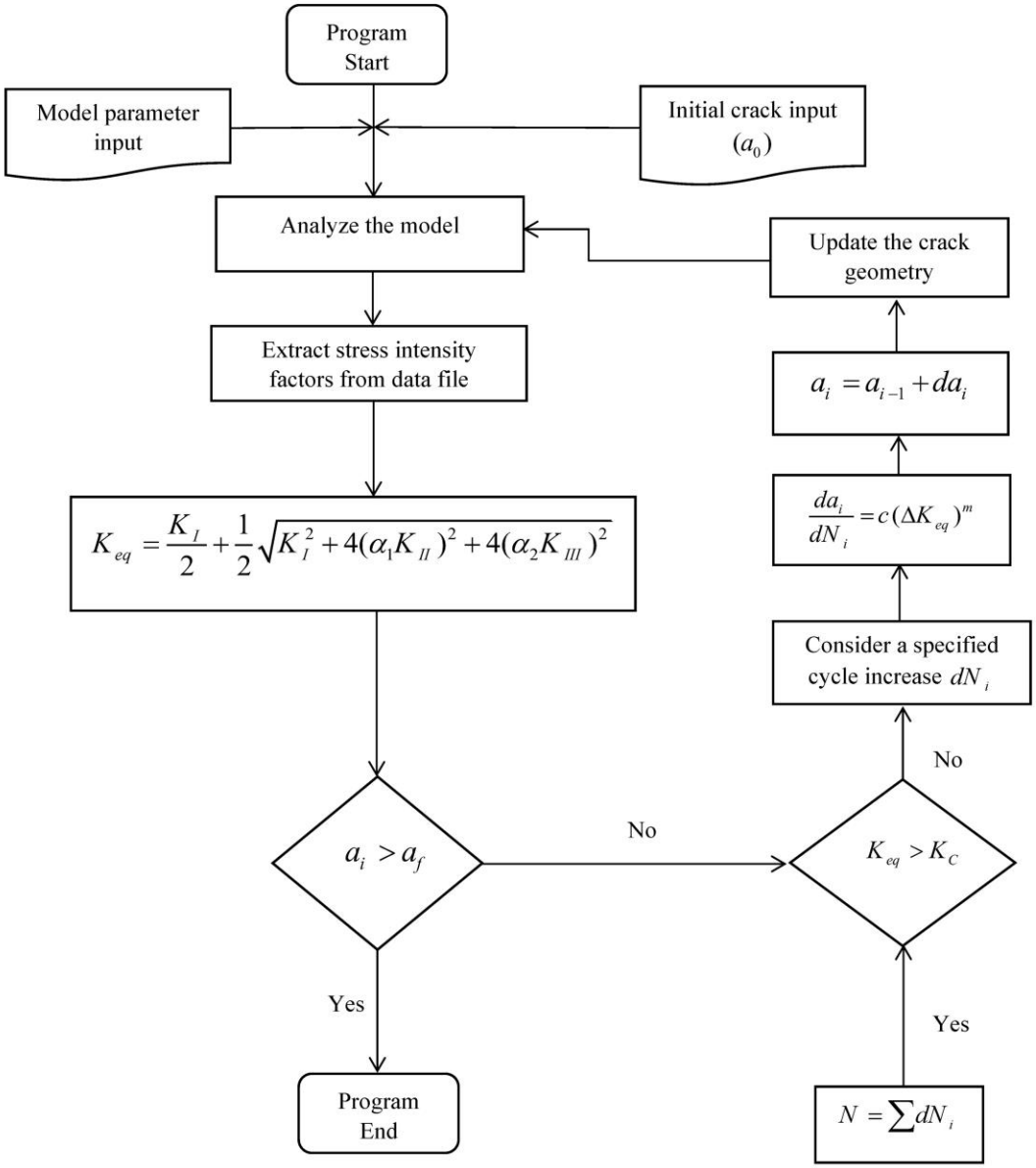

Figure 1- Flowchart of high cycle fatigue XFEM script.

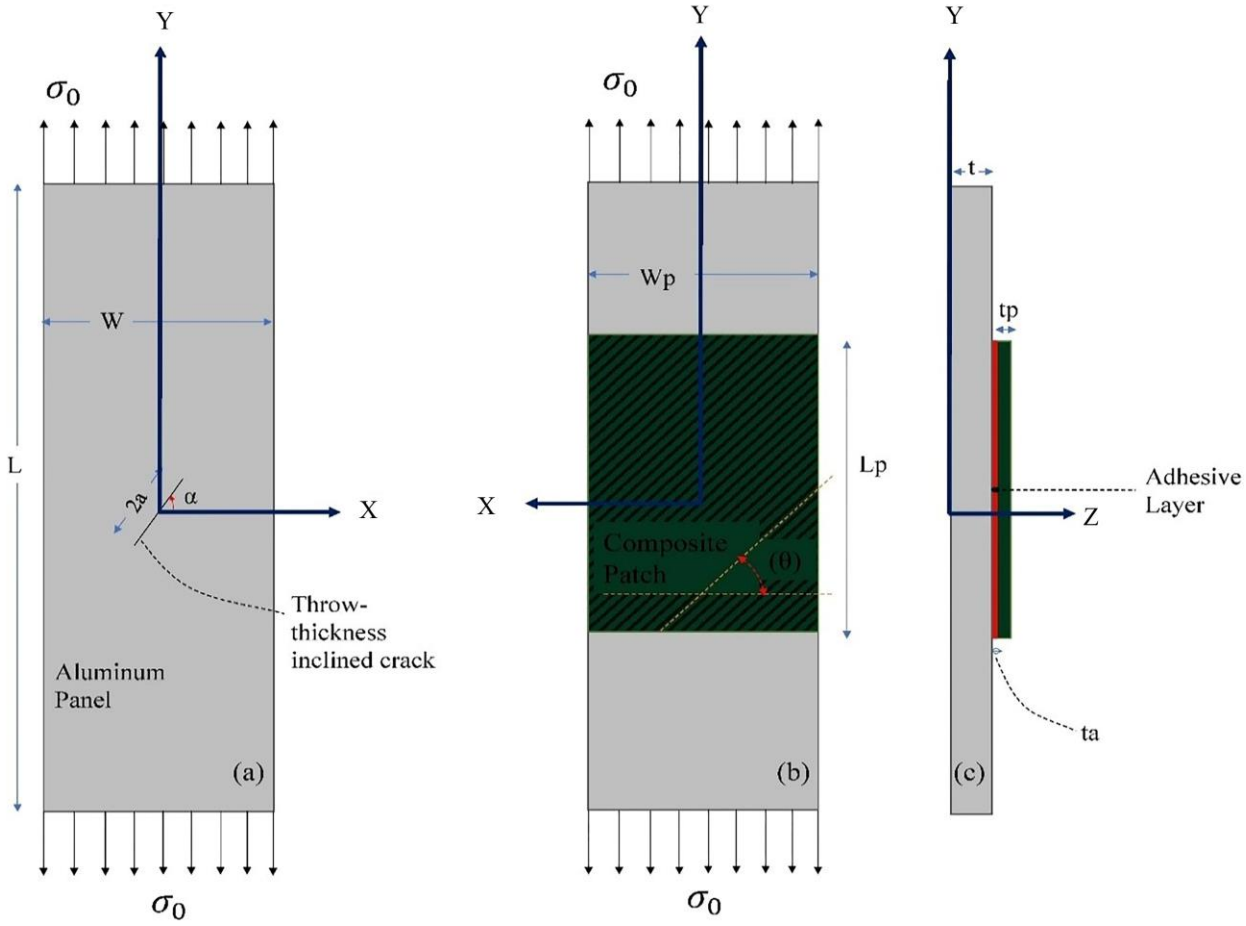

Figure 2- Geometry of the problem; a) front view b) back view c) side view.

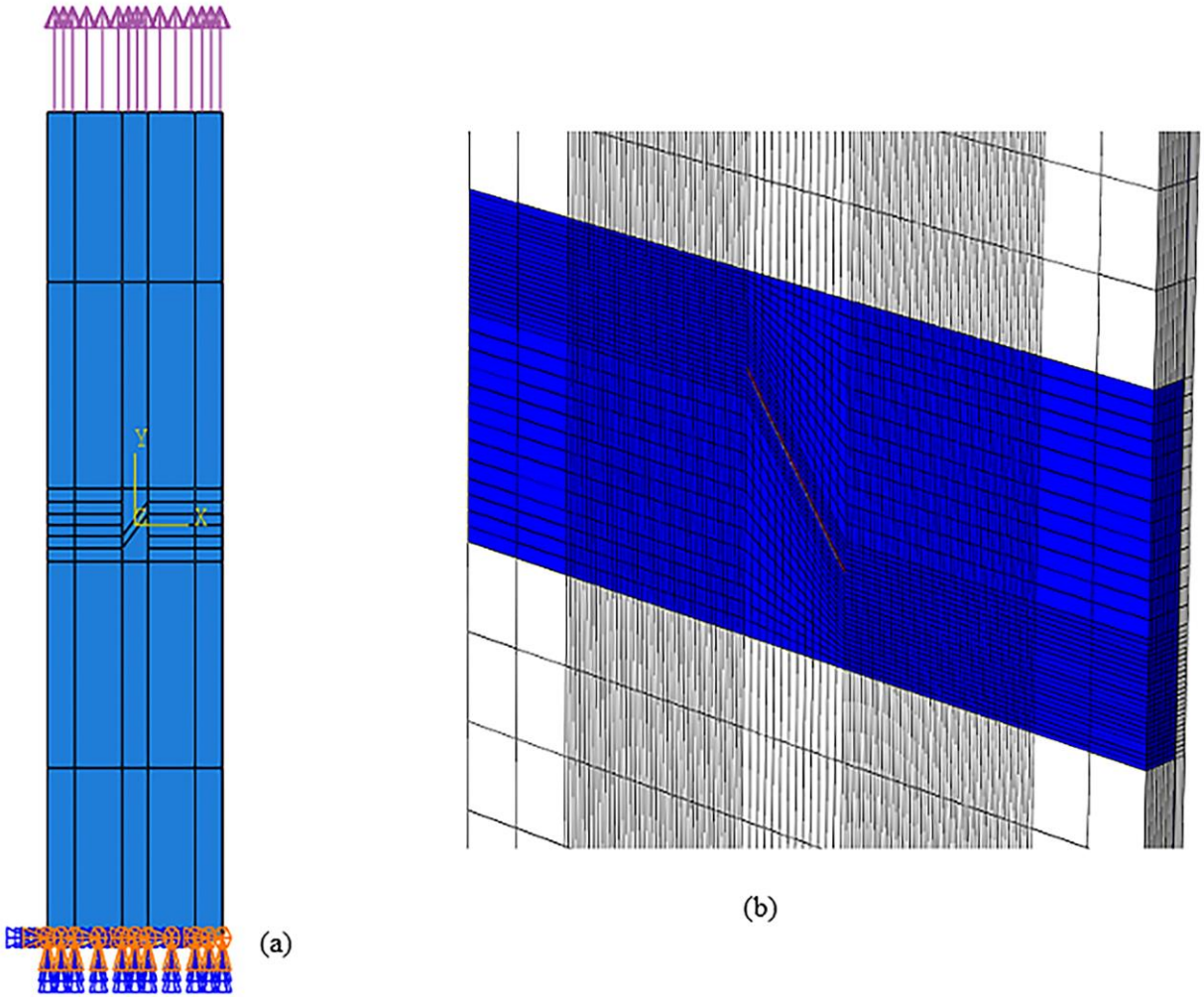

Figure 3- View of 3D model (a), and refined mesh around the crack(b)

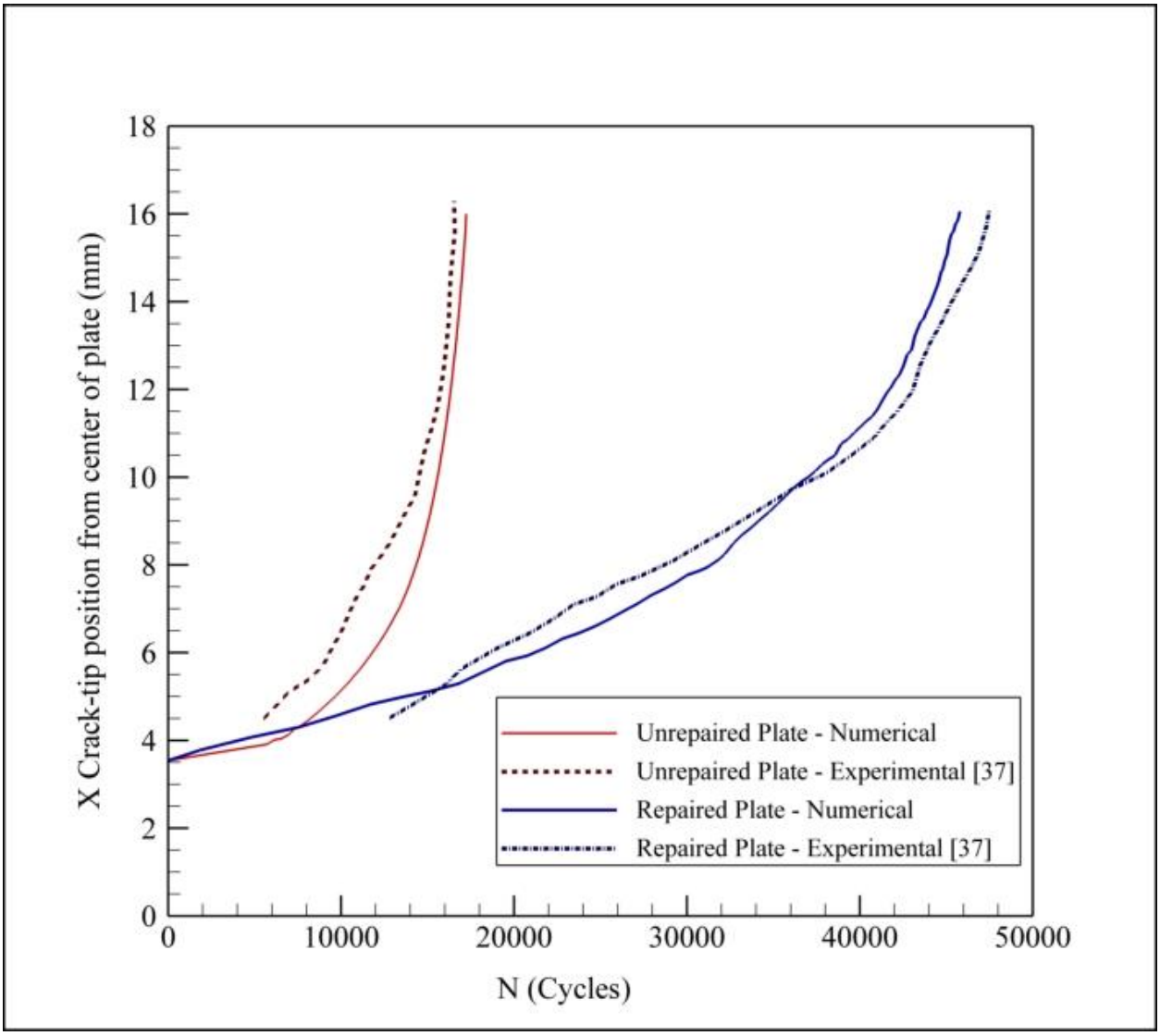

Figure 4- Comparison of crack growth behavior obtained from this study with experimental reference [37] for un-patched plate and patched plate with $[-75]_4$ lay-up patch and FM 73 adhesive.

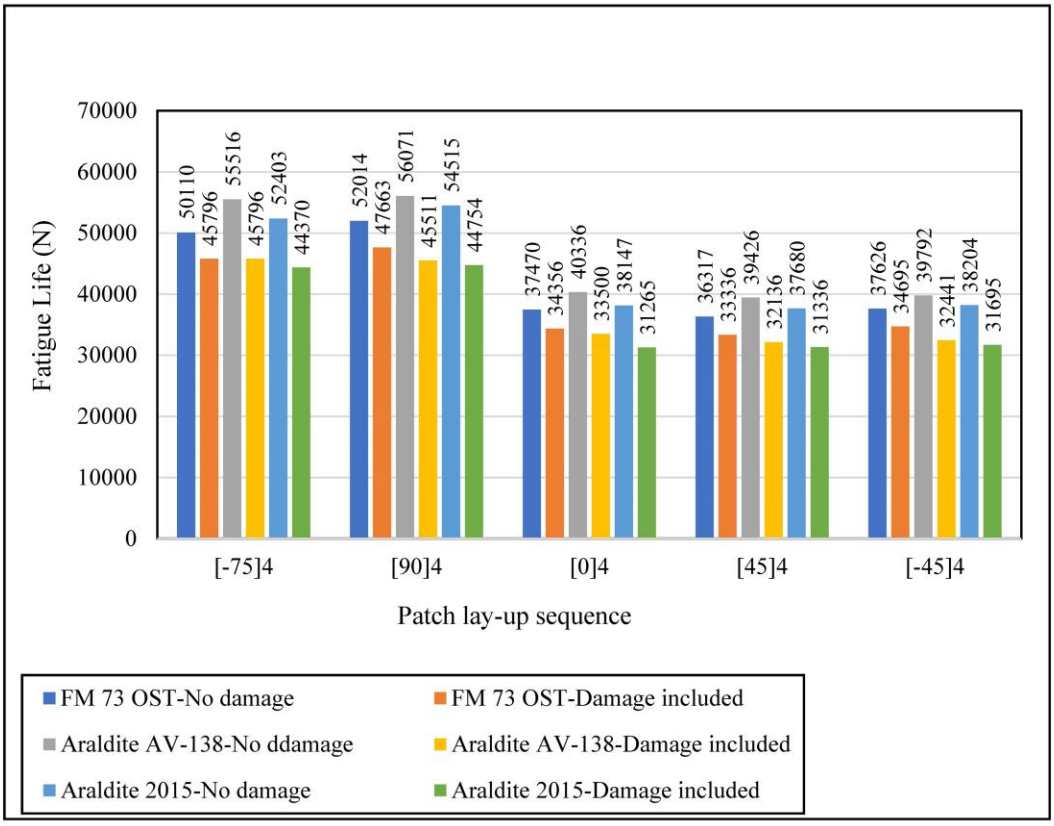

Figure 5- Fatigue life (number of cycles) prediction of the plate with different lay-up patches and adhesives

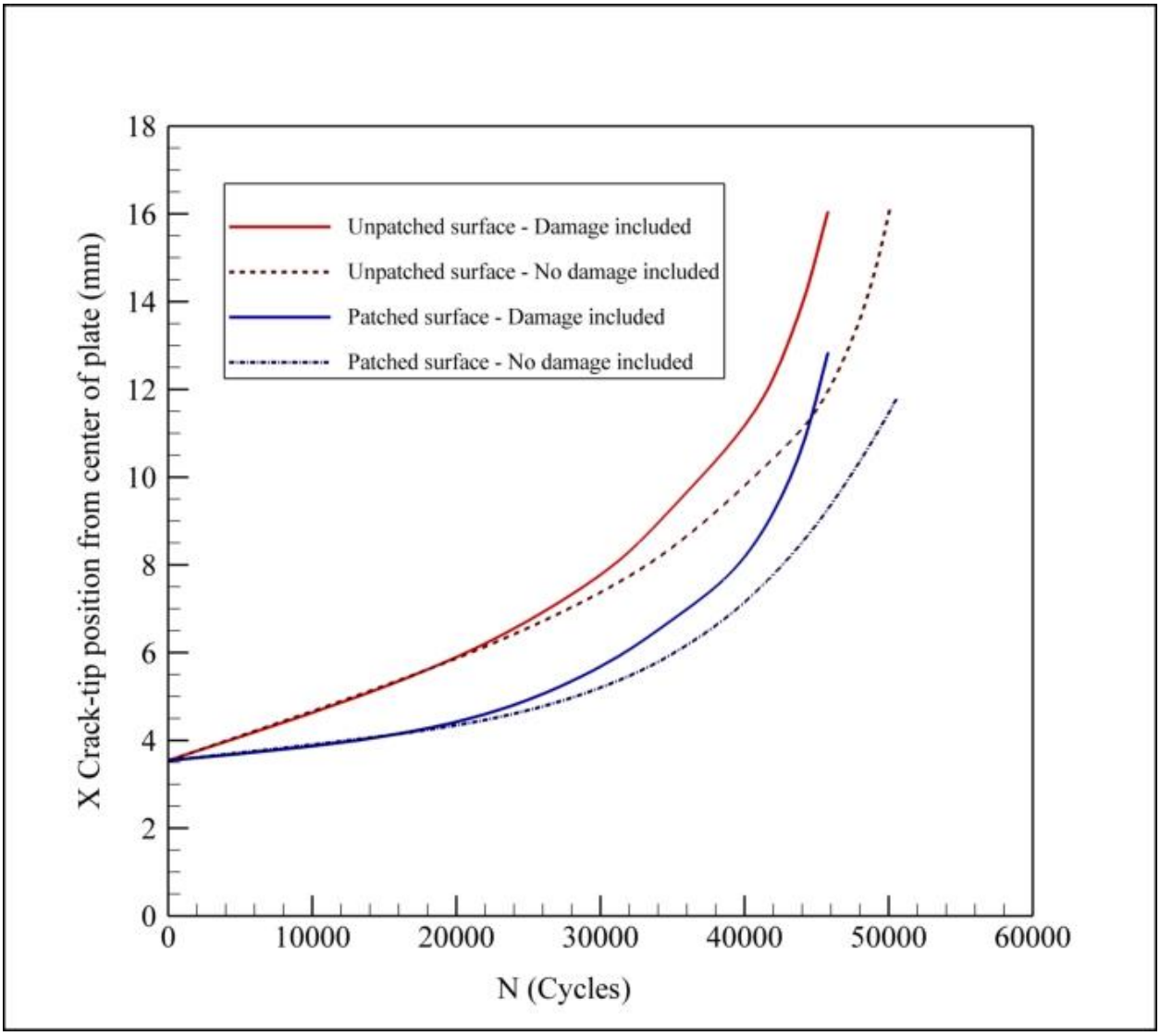

Figure 6- Comparison of a-N curves on patched and un-patched surfaces obtained from damage-including and no-damage models for patched plate with $[-75]_4$ lay-up patch and FM 73 adhesive.

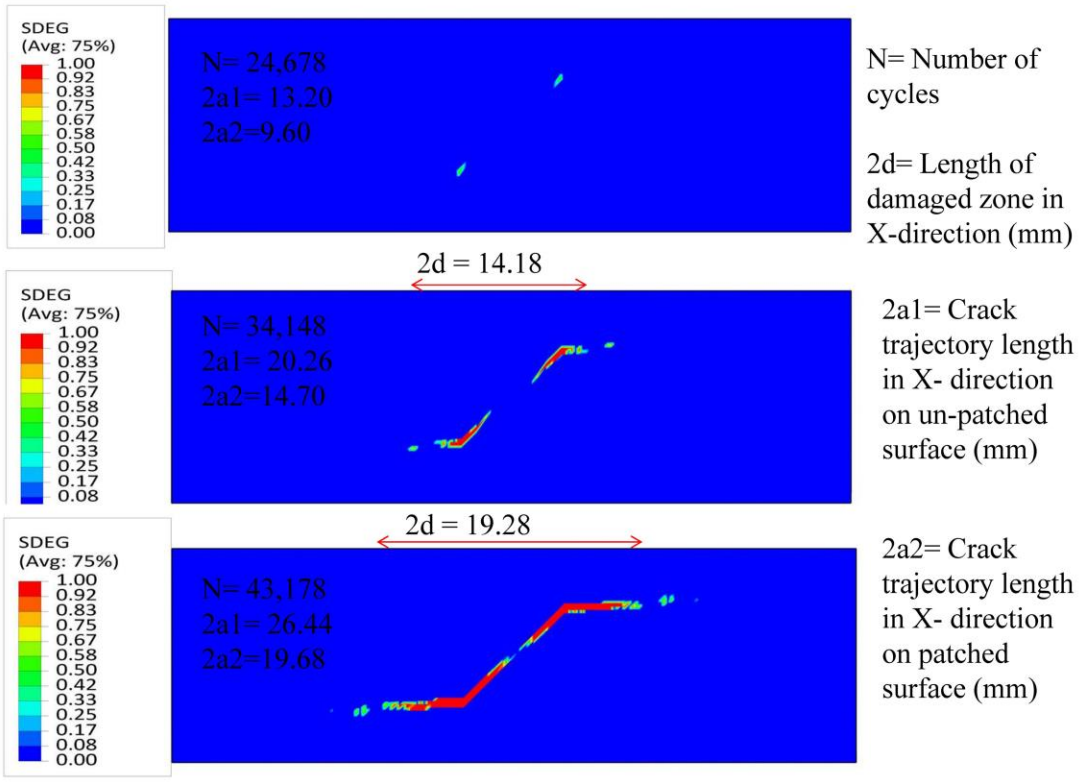

Figure 7- Damage evolution in adhesive layer for patched plate with $[-75]_4$ lay-up patch with FM 73 adhesive.

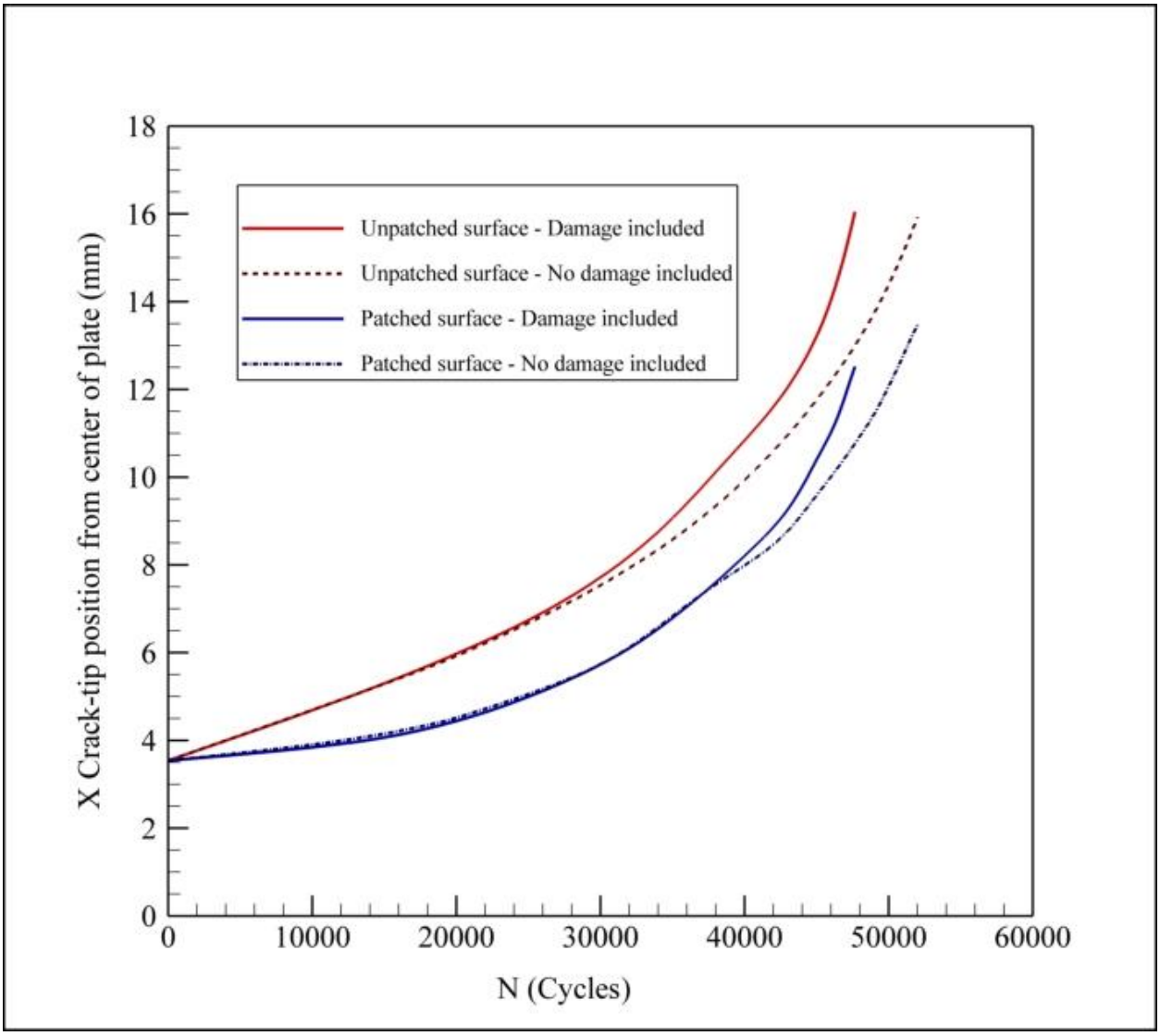

Figure 8- Comparison of a-N curves on patched and un-patched surfaces obtained from damage-including and no-damage models for patched plate with $[90]_4$ lay-up patch and FM 73 adhesive.

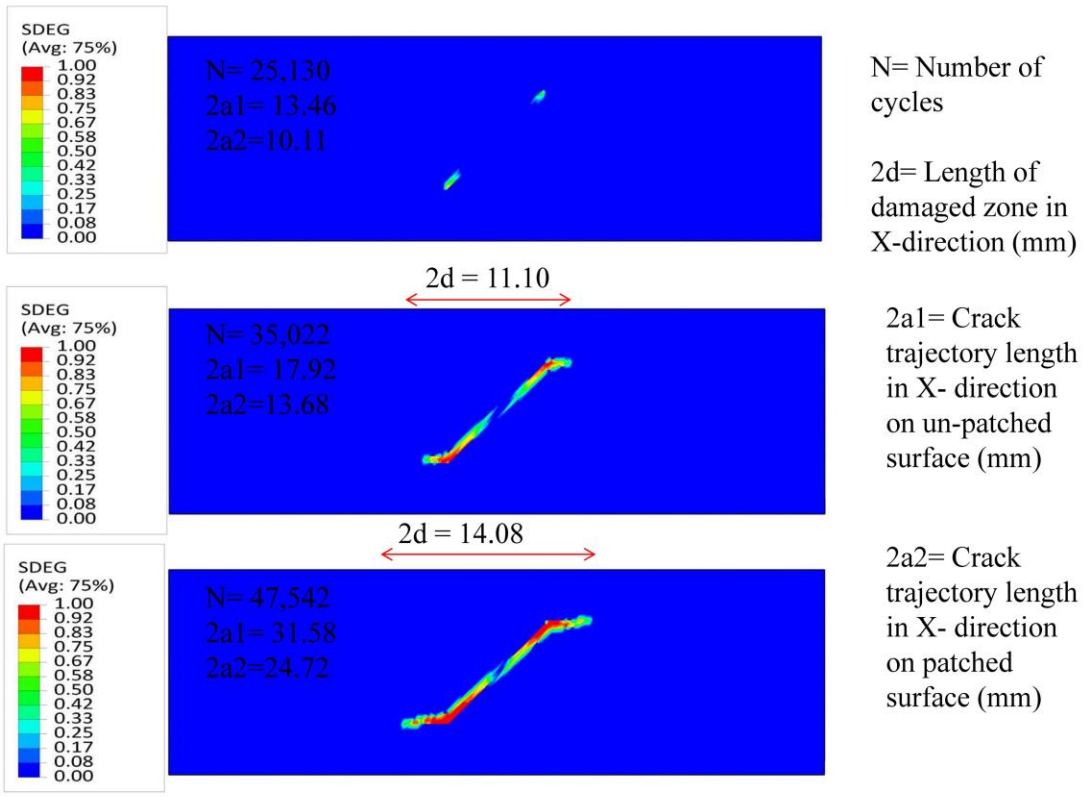

Figure 9- Damage evolution in adhesive layer for patched plate with $[90]_4$ lay-up patch with FM 73 adhesive.

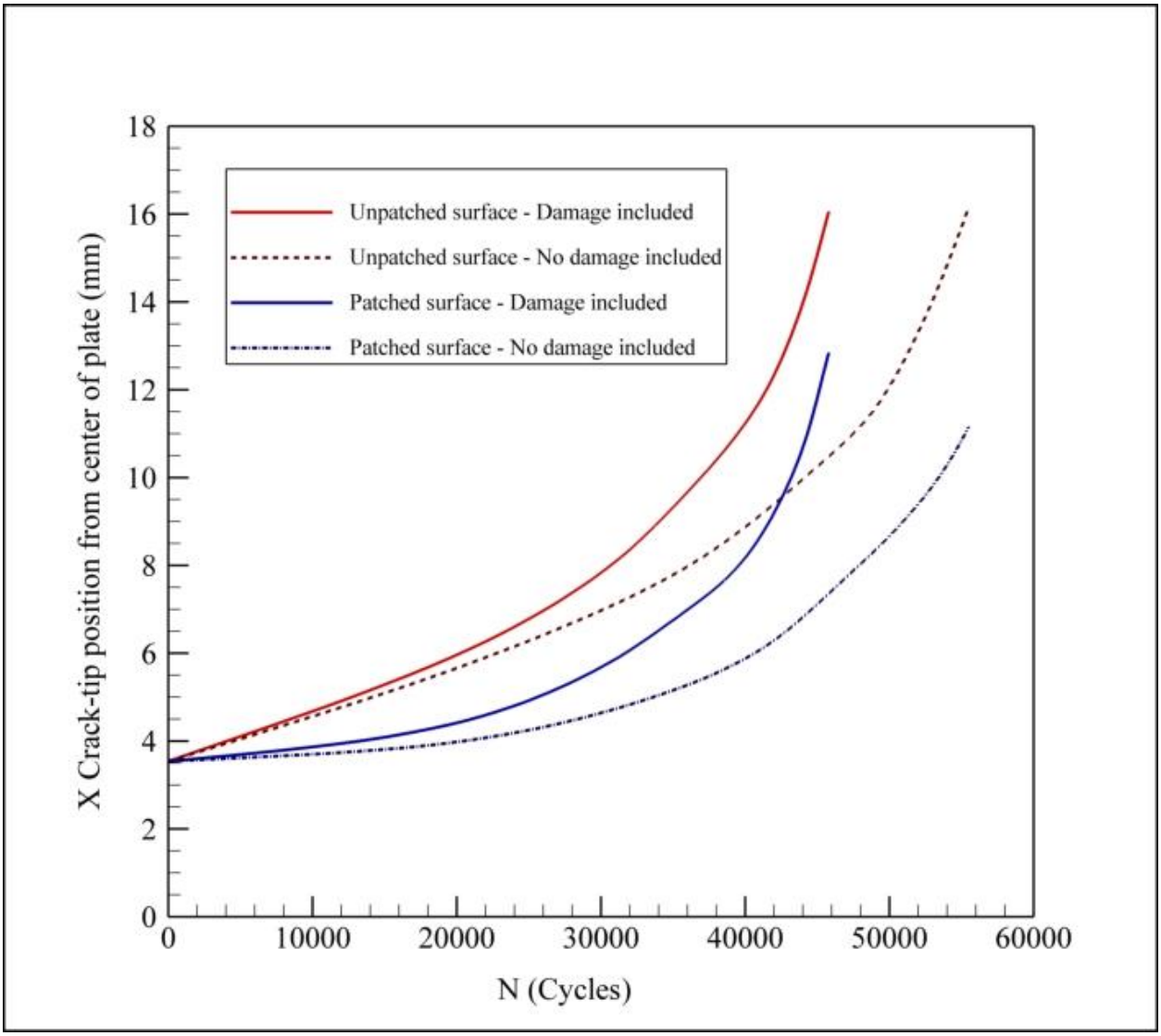

Figure 10- Comparison of a-N curves on patched and un-patched surfaces obtained from damage-including and no-damage models for patched plate with $[-75]_4$ lay-up patch and AV138 adhesive.

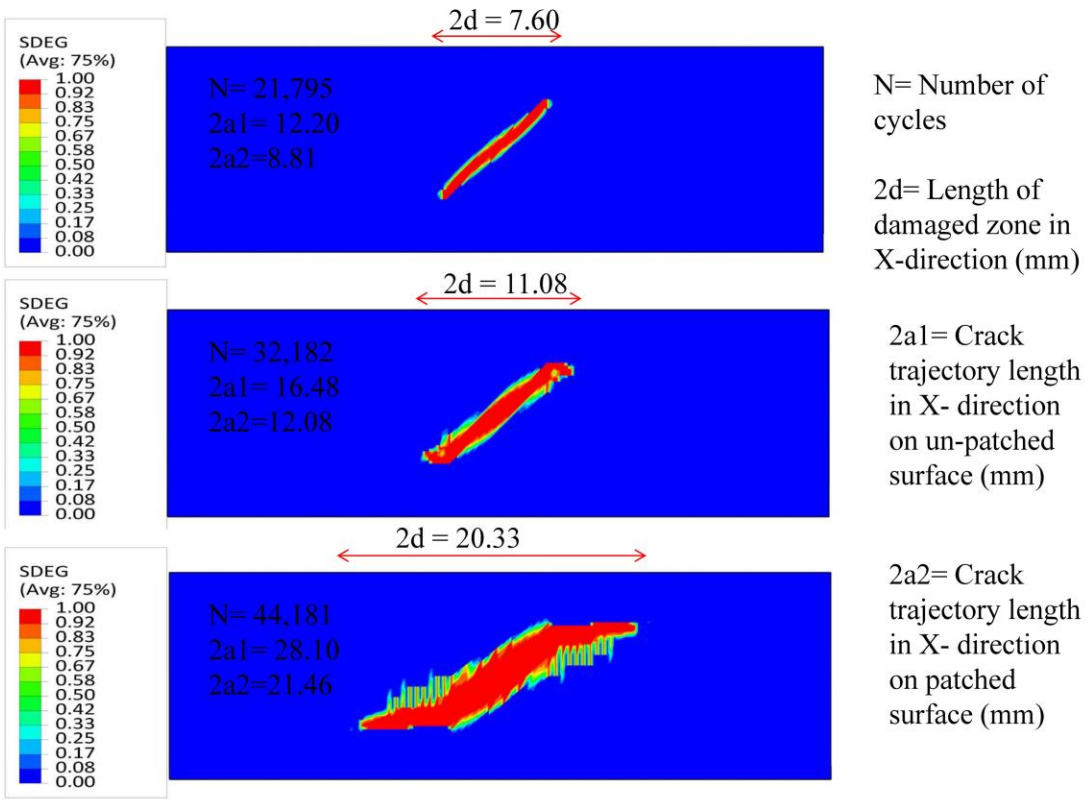

Figure 11- Damage evolution in adhesive layer for patched plate with $[-75]_4$ lay-up patch with AV138 adhesive.

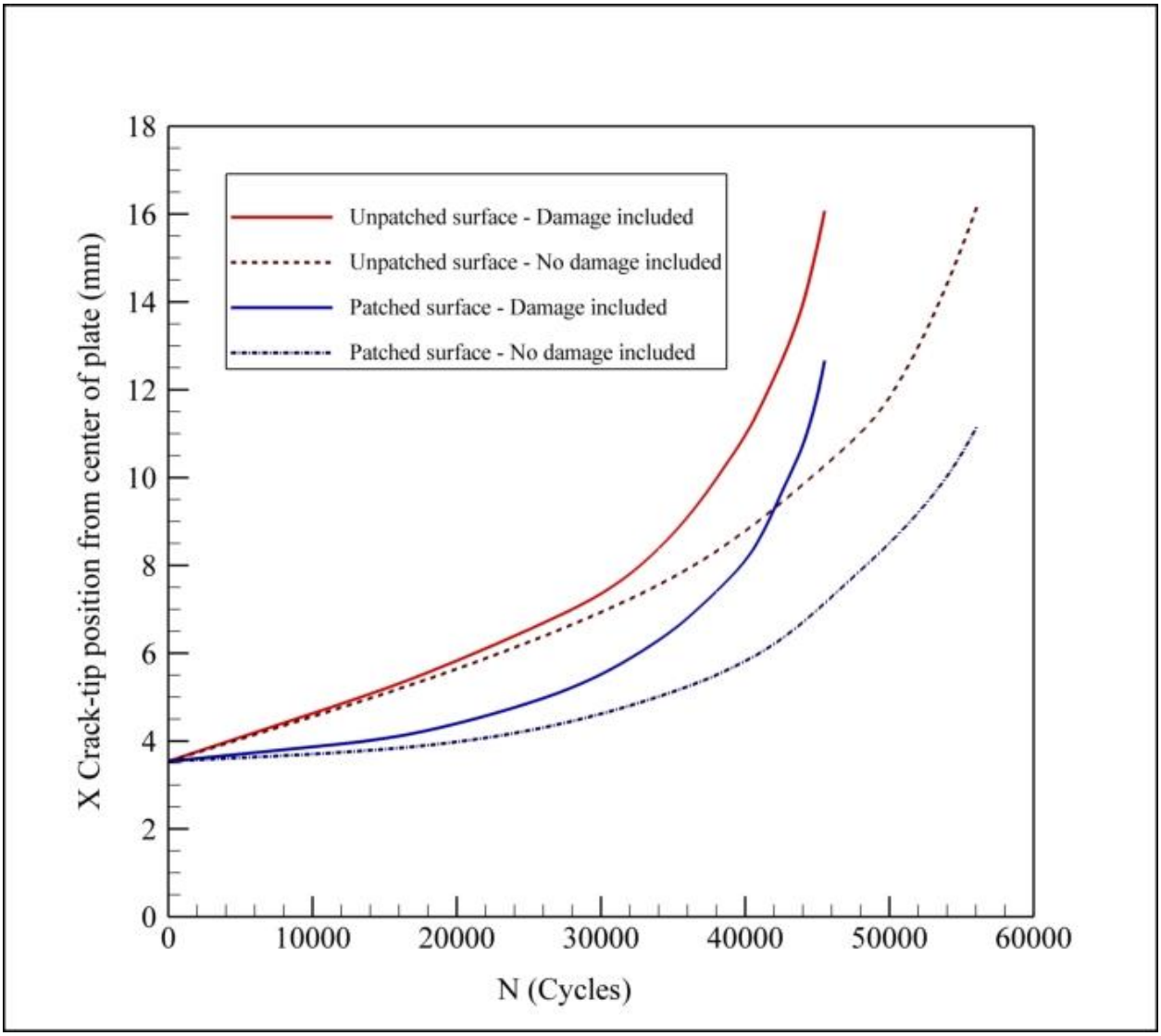

Figure 12- Comparison of a-N curves patched and un-patched surfaces obtained from damage-including and no-damage models for patched plate with $[90]_4$ lay-up patch and AV138 adhesive.

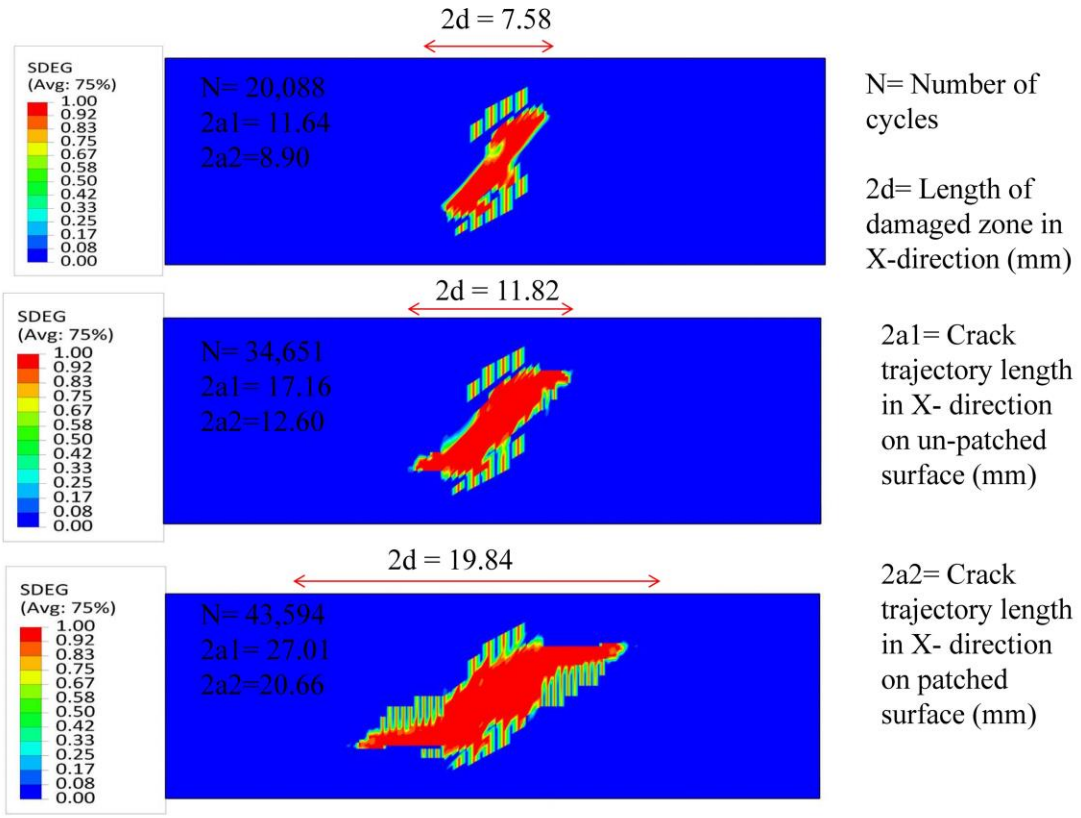

Figure 13- Damage evolution in adhesive layer for patched plate with $[90]_4$ lay-up patch with AV138 adhesive.

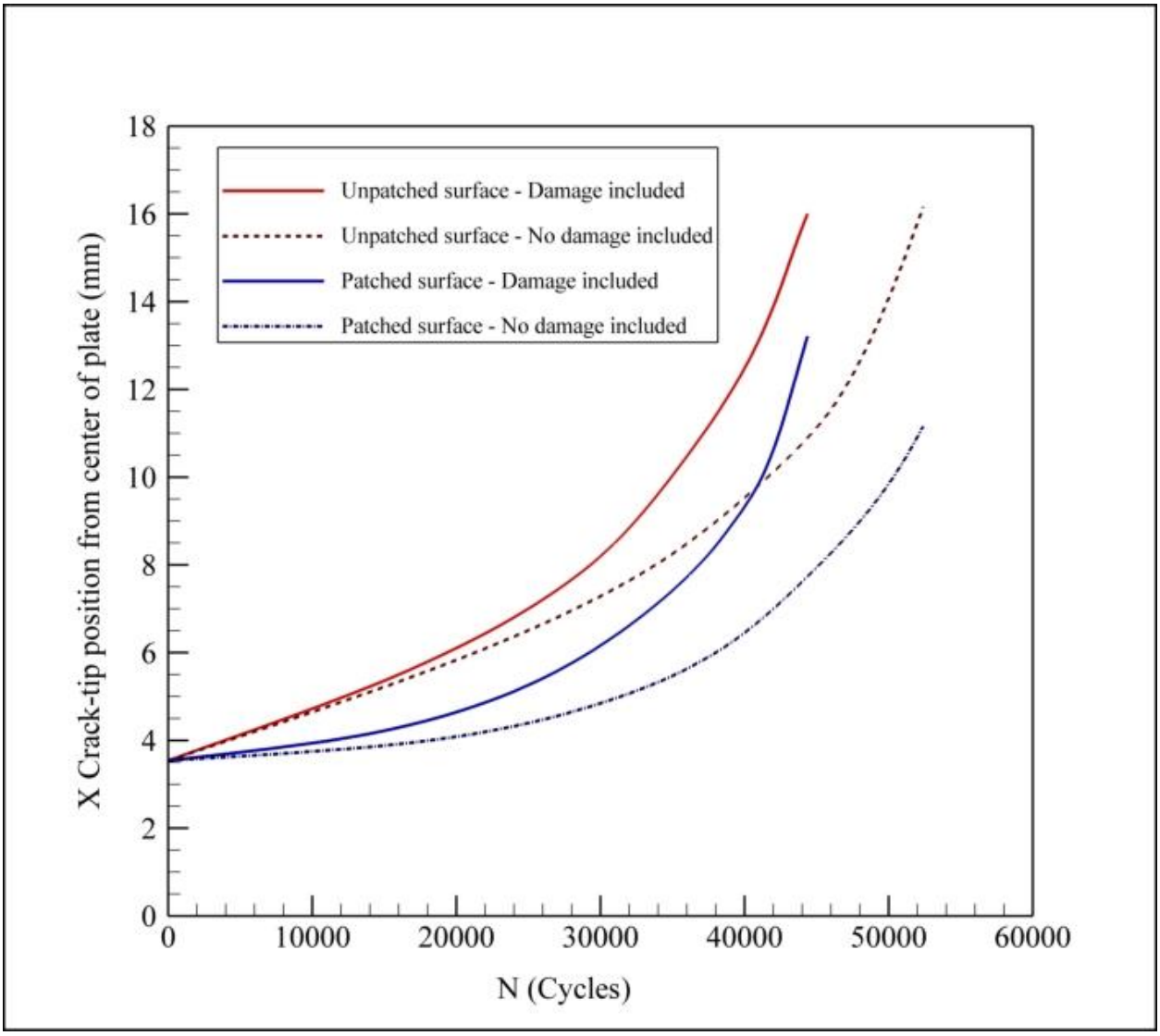

Figure 14- Comparison of a-N curves on patched and un-patched surfaces obtained from damage-including and no-damage models for patched plate with $[-75]_4$ lay-up patch and 2015 adhesive.

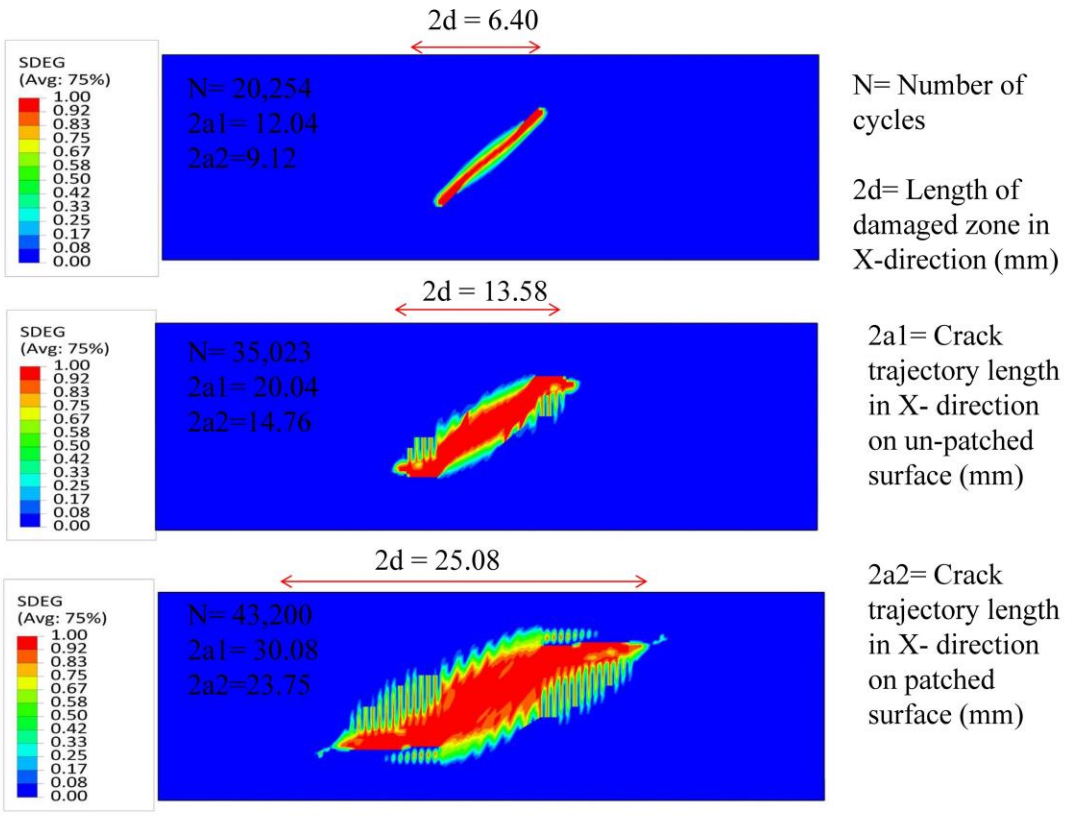

Figure 15- Damage evolution in adhesive layer for patched plate with $[-75]_4$ lay-up patch with 2015 adhesive.

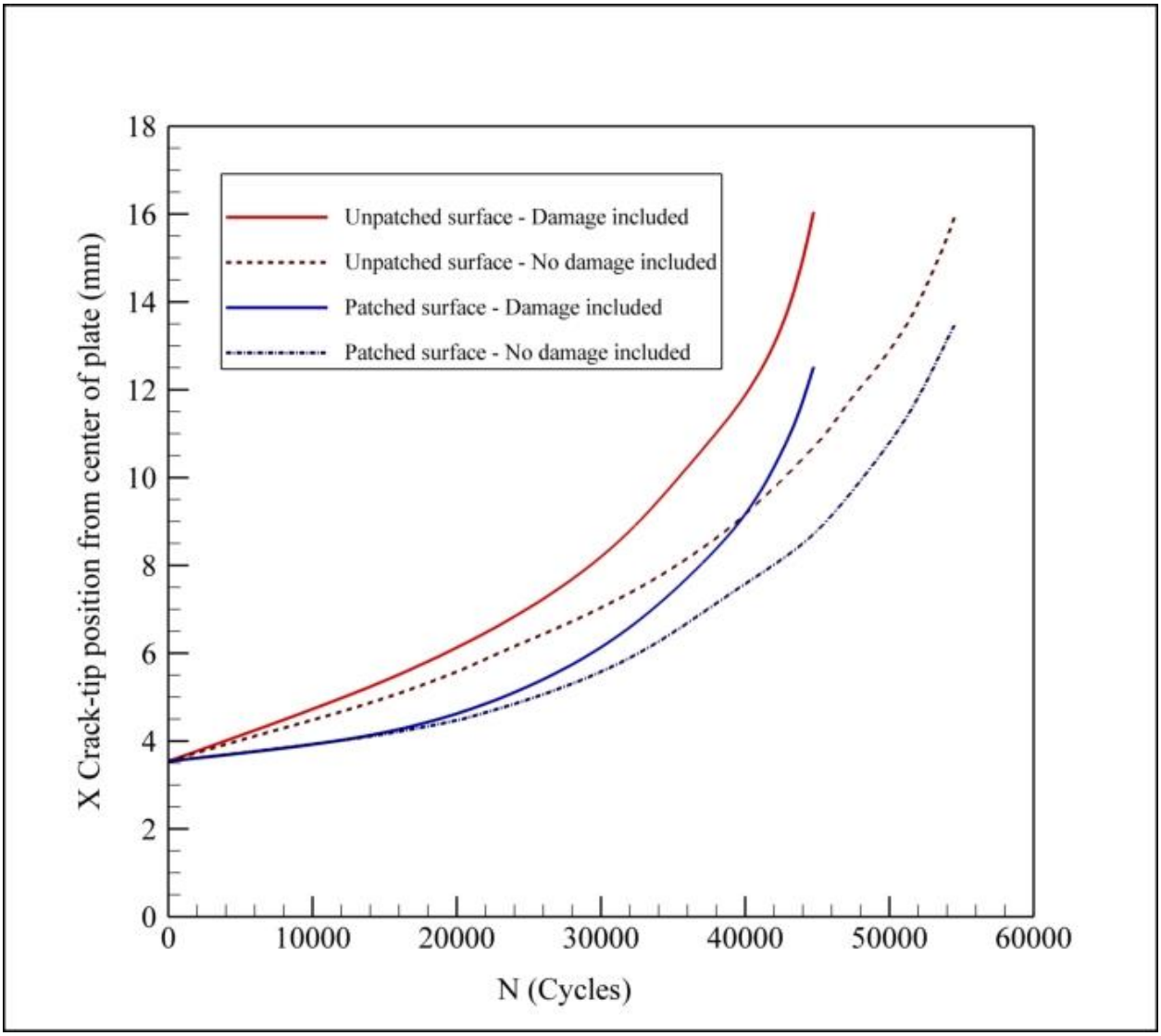

Figure 16- Comparison of a-N curves on patched and un-patched surfaces obtained from damage-including and no-damage models for patched plate with $[90]_4$ lay-up patch and 2015 adhesive.

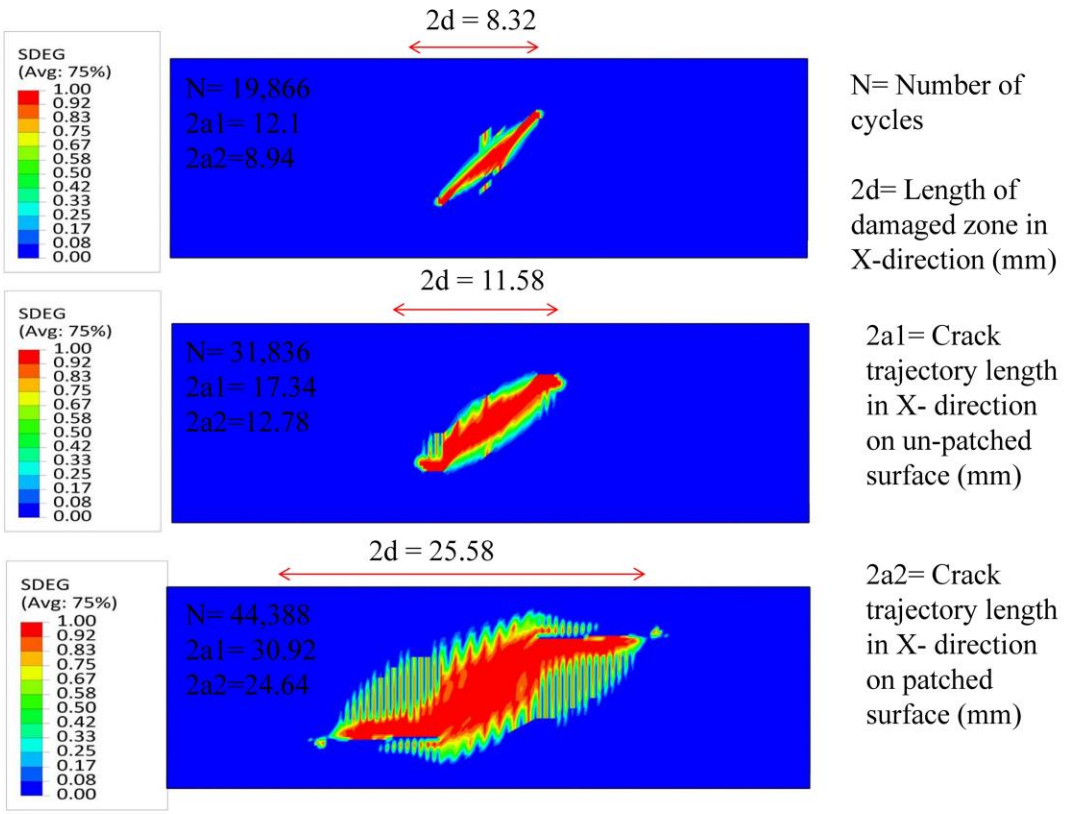

Figure 17- Damage evolution in adhesive layer for patched plate with $[90]_4$ lay-up patch with 2015 adhesive.

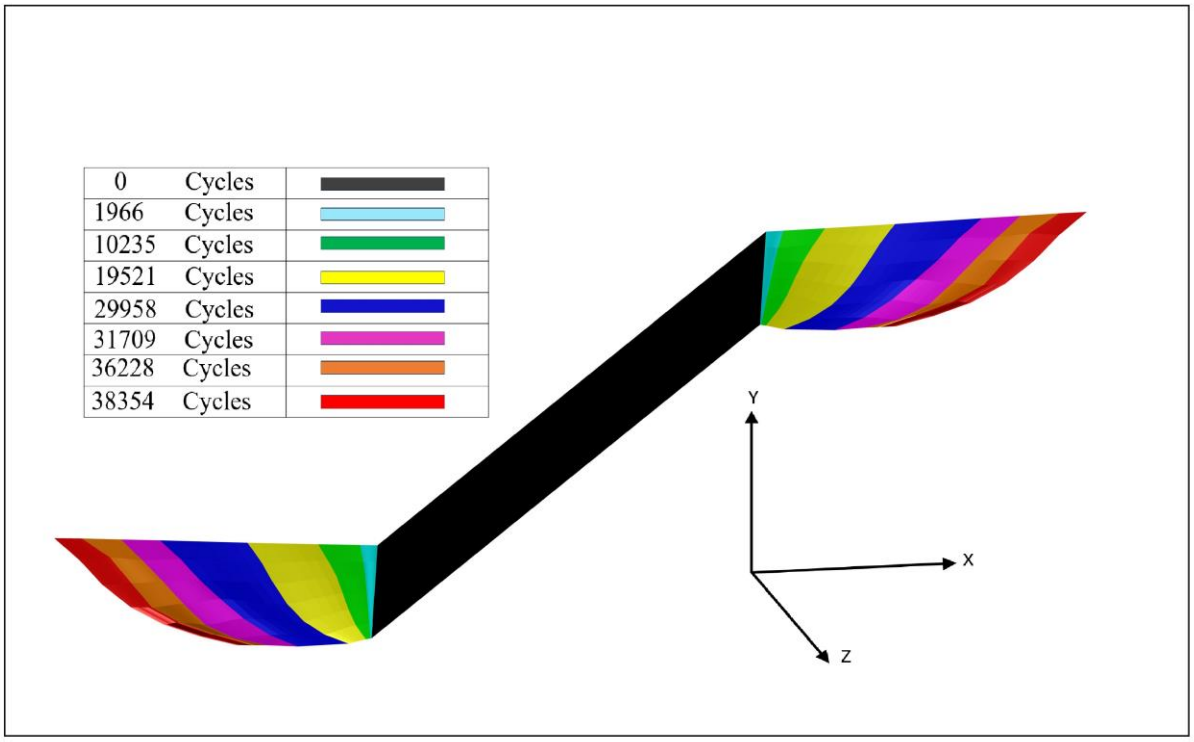

Figure 18- Isometric view of crack in different loading cycles obtained from no-damage model.

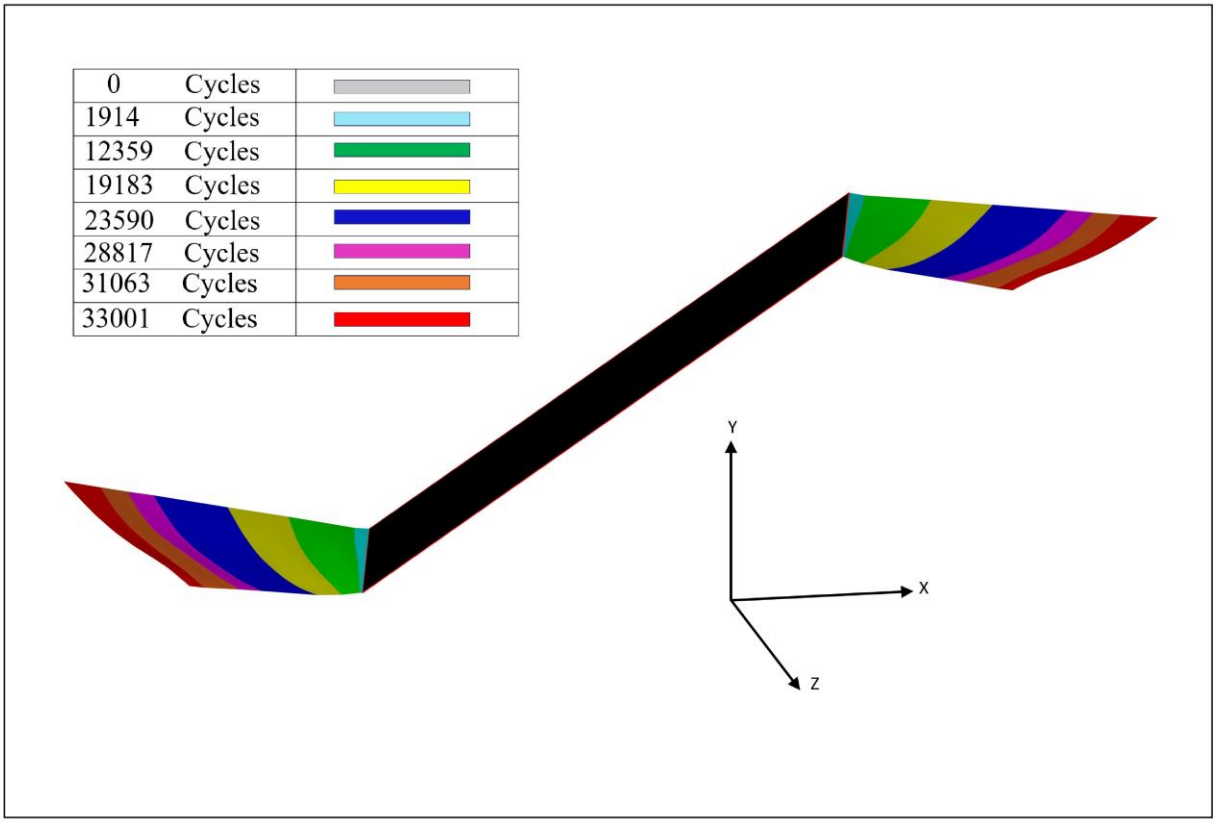

Figure 19- Isometric view of crack in different loading cycles obtained from CZM model.

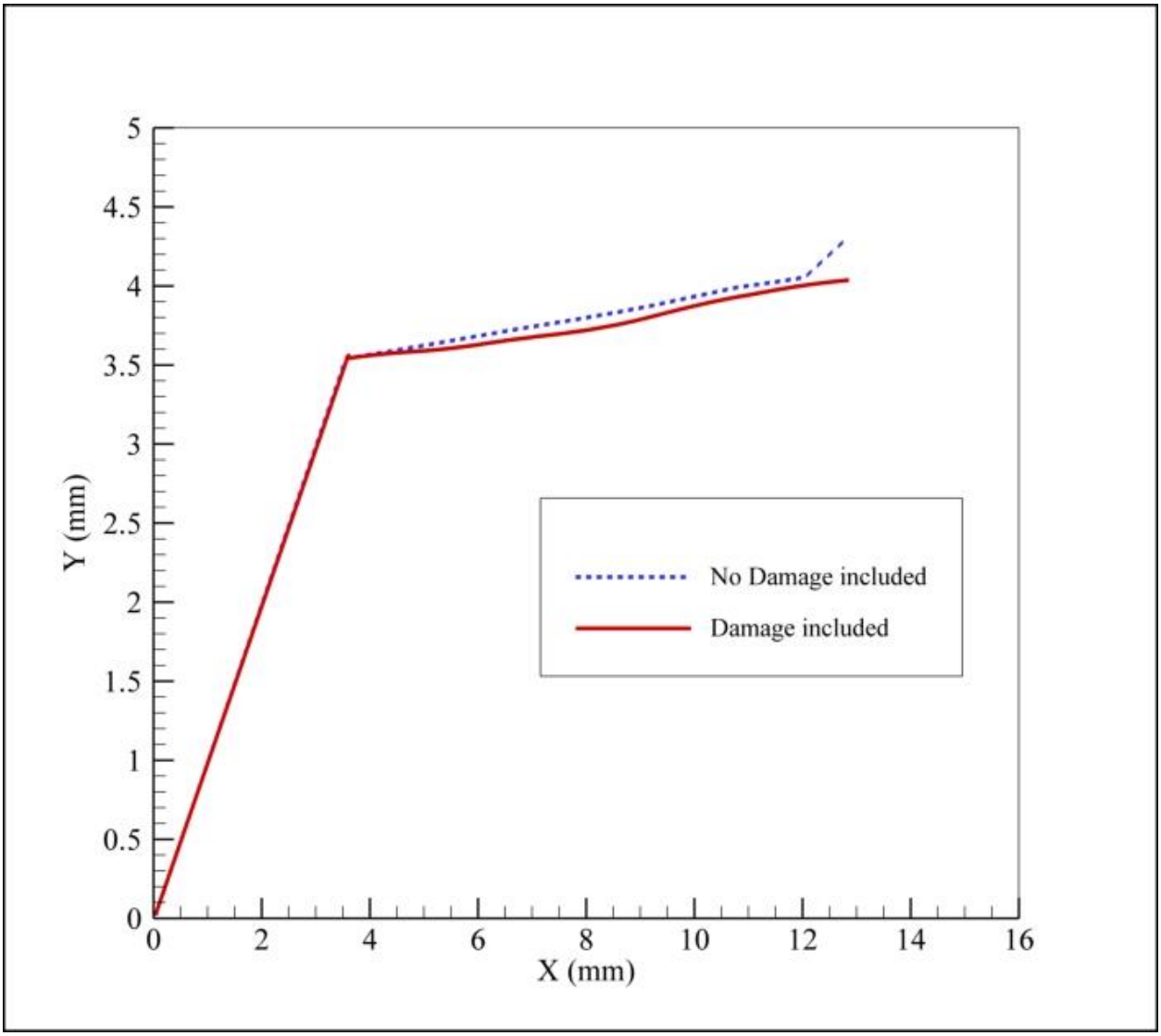

Figure 20- Crack trajectory on metal surface of patched plate with $[-75]_4$ lay-up

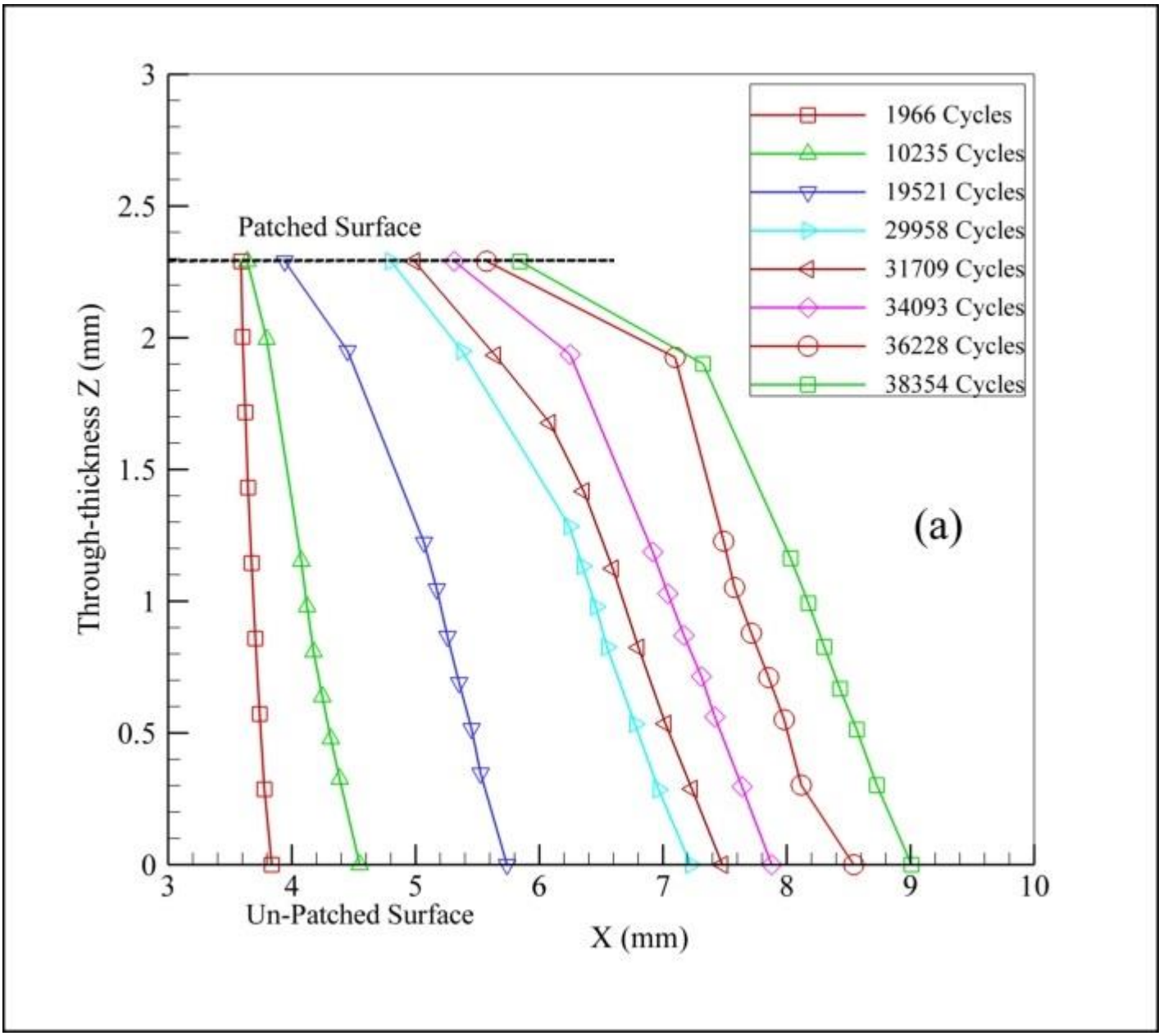
1966 Cycles
10235 Cycles
19521 Cycles
29958 Cycles
31709 Cycles
34093 Cycles
36228 Cycles
38354 Cycles
Patched Surface
Un-Patched Surface
Through-thickness Z (mm)
X (mm)
(a)
0
0.5
1
1.5
2
2.5
3
3
4
5
6
7
8
9
10

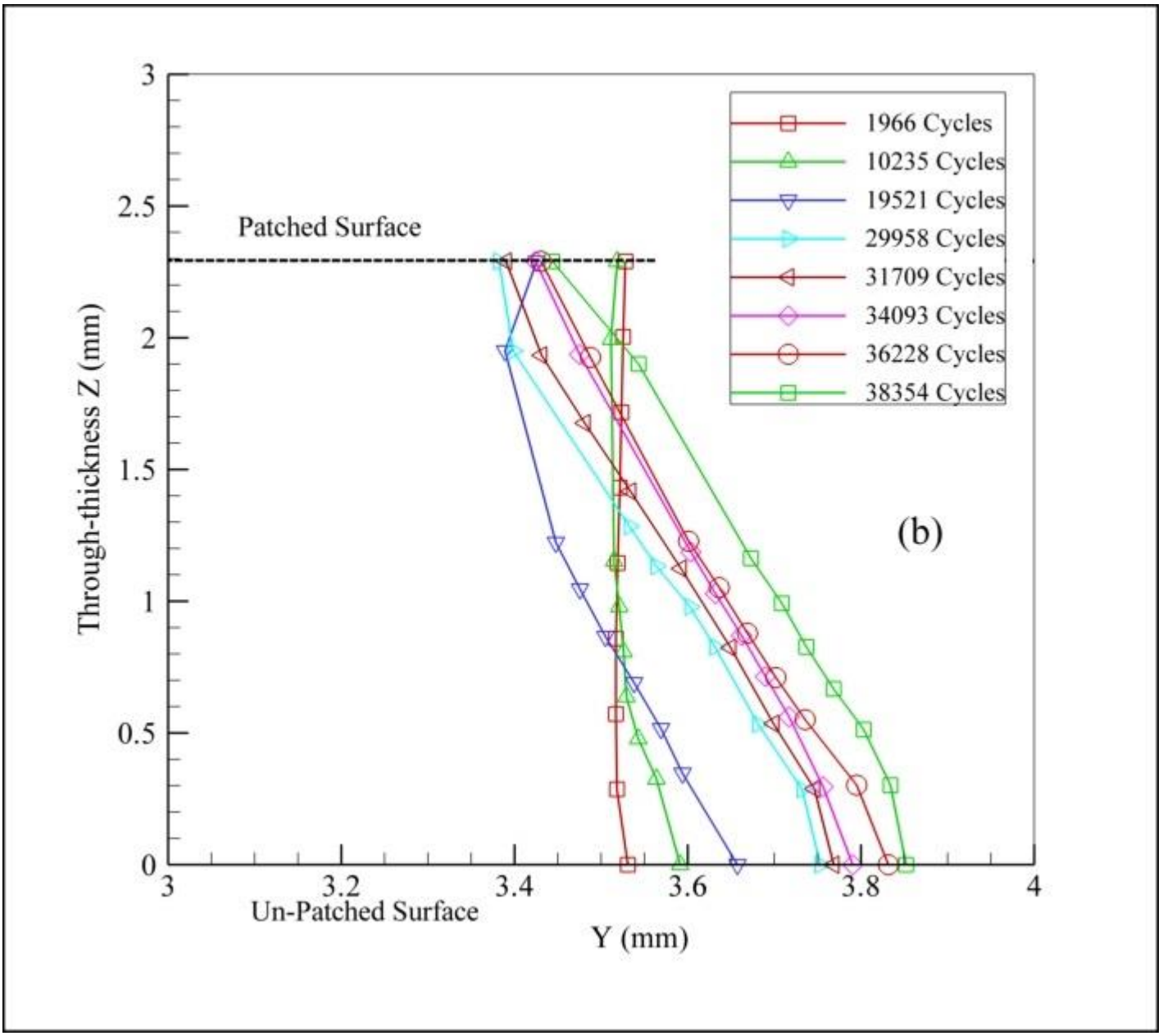

Figure 21- Crack front development for patched plate with $[-75]_4$ patch lay-up at: a) XZ; b) YZ plane under different fatigue cycle numbers obtained from no-damage model.

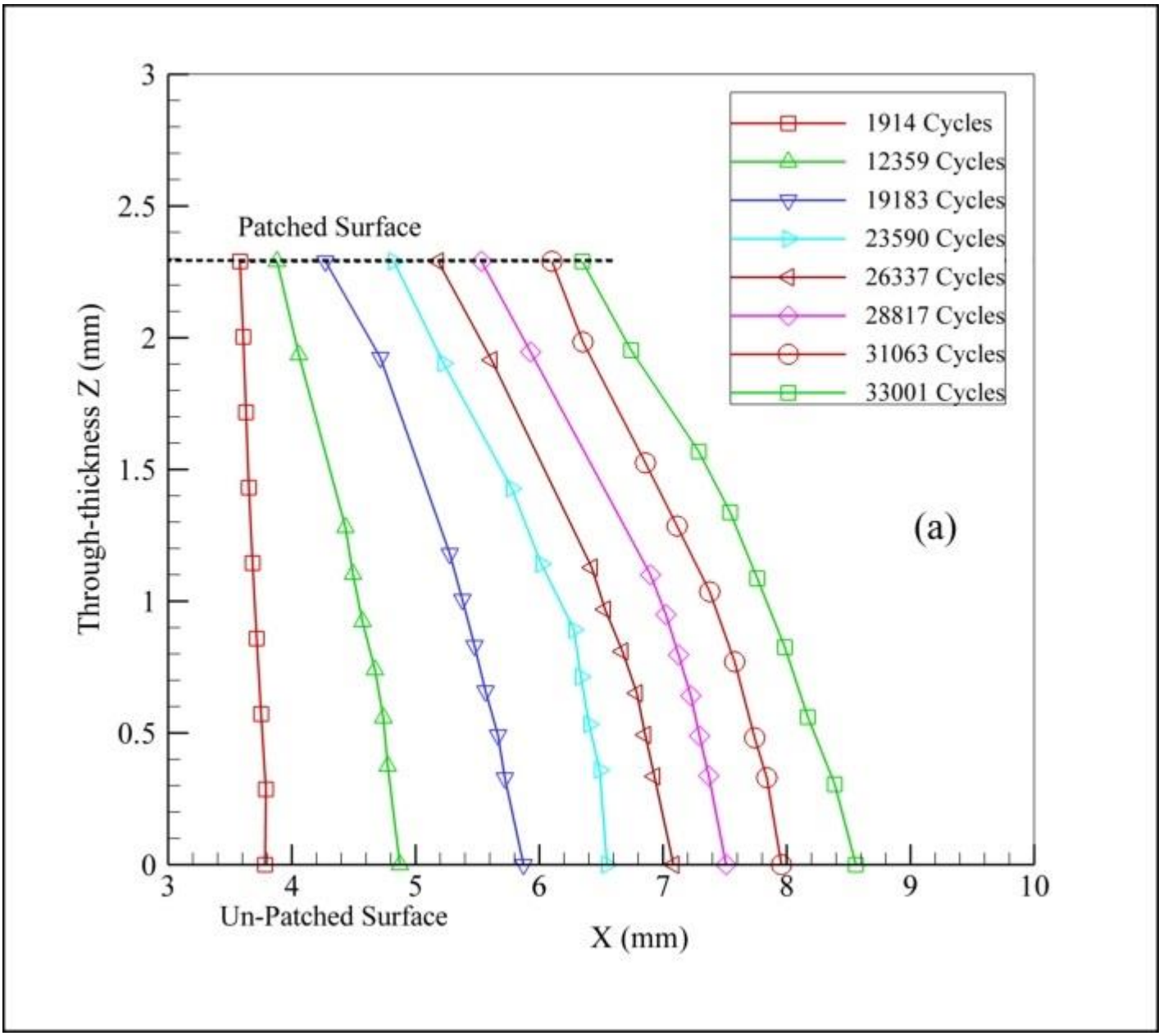
Through-thickness Z (mm)
X (mm)
Patched Surface
Un-Patched Surface
1914 Cycles
12359 Cycles
19183 Cycles
23590 Cycles
26337 Cycles
28817 Cycles
31063 Cycles
33001 Cycles
(a)
0
0.5
1
1.5
2
2.5
3
3
4
5
6
7
8
9
10

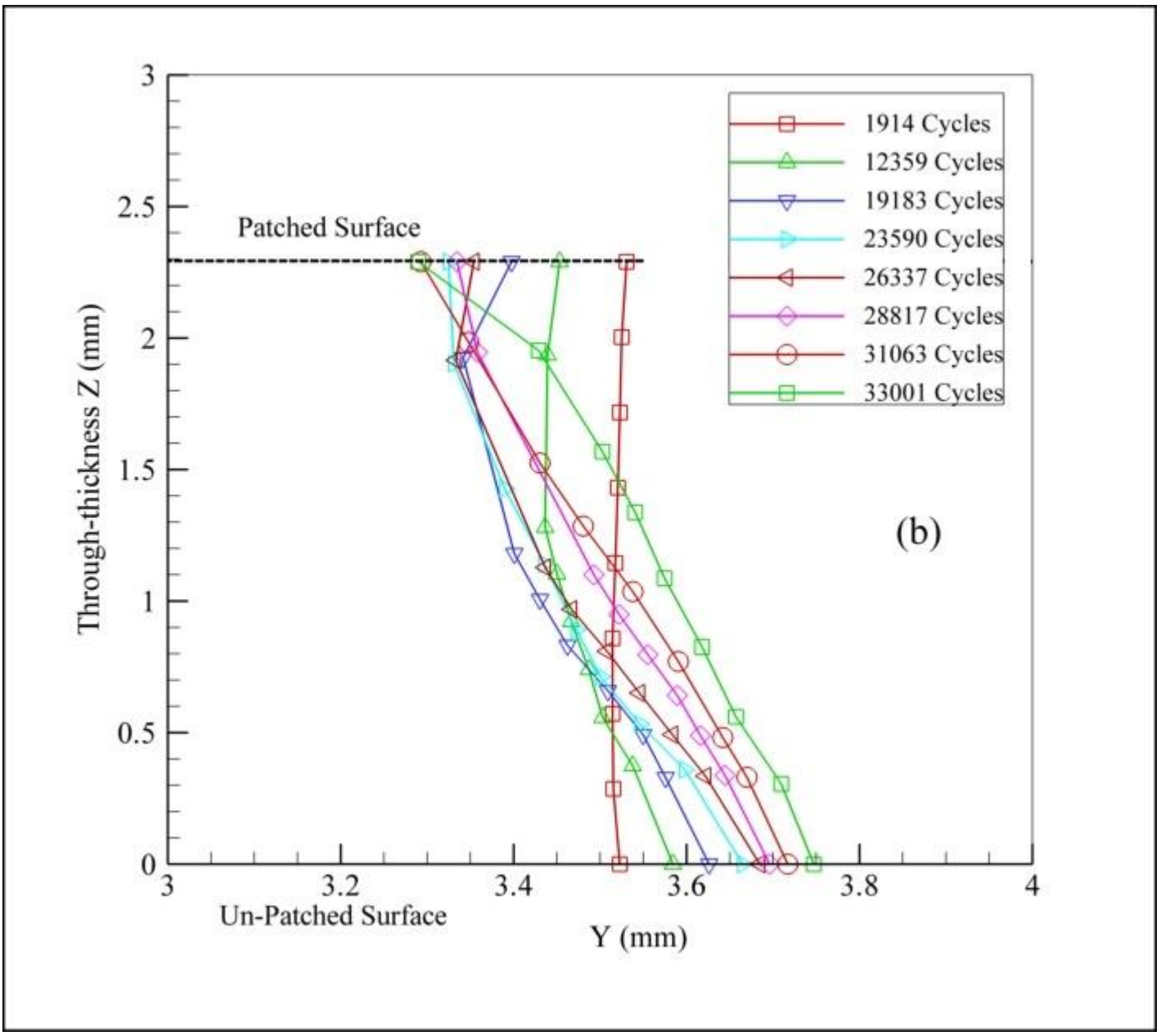

Figure 22- Crack front development for patched plate with $[-75]_4$ patch lay-up at: a) XZ; b) YZ plane under different fatigue numbers obtained from CZM model.

Authors' Biographies

Javad Eidan, a Ph.D. candidate in structural engineering at Amir Kabir University of Technology (Tehran Polytechnic), Tehran, Iran. Javad has a strong interest in the computational mechanics of structures. His field of interest is strengthening structures against fatigue loading using robust effective methods, utilizing novel economical materials.

Mohammad Zaman Kabir is a professor of Structures and Solid Mechanics at the Department of Civil and Environmental Engineering at Amir Kabir University of Technology in Tehran, Iran. Pro. Kabir earned his Ph.D. in 1995 from the Solid Mechanics Division at the Department 716 of Civil Engineering at the University of Waterloo in Ontario, Canada, where his research focused on the stability of thin-walled laminated composite members. Prof. Kabir has authored 718 numerous papers on topics such as composite structures, structural stability, structural 719 optimization, prefabricated sandwich panels, and retrofitting structures using FRP fabrics. His 720 current research interests include strengthening structures under excessive loading, innovative 721 materials for structures, lightweight structures, and the application of 3D printing in the civil 722 engineering industry.